Research Paper

Mapping of spinal interneurons involved in regulation of the lower urinary tract in juvenile male rats

S.V. Karnup*, W.C. De Groat

Department of Pharmacology and Chemical Biology, University of Pittsburgh, Pittsburgh, PA, 15213, United States

A B S T R A C T

Coordination between the urinary bladder (BL) and external urethral sphincter (EUS) is necessary for storage and elimination of urine. In rats interneuronal circuits at two levels of the spinal cord (i.e., L6-S1 and L3-L4) play an important role in this coordination. In the present experiments retrograde trans-synaptic transport of pseudorabies virus (PRV) encoding fluorescent markers (GFP and RFP) was used to trace these circuits. To examine the relative localization of EUS-related and BL-related interneuronal populations we injected PRV-GFP into the EUS and PRV-RFP into the BL wall. The PRV infected populations of spinal interneurons were localized primarily in the dorsal commissure (DCM) of L6/S1 and in a hypothesized lumbar spinal coordinating center (LSCC) in L3/L4 above and lateral to central canal (CC). At both sites colocalization of markers occurred in a substantial number of labeled interneurons indicating concomitant involvement of these double-labelled neurons in the EUS- and BL-circuits and suggesting their role in EUS-BL coordination. Intense GFP or RFP fluorescent was detected in a subpopulation of cells at both sites suggesting that they were infected earlier and therefore likely to represent first order, primary interneurons that directly synapse with output neurons. Larger numbers of weakly fluorescent neurons that likely represent second order interneurons were also identified. Within the population of EUS-related first order interneurons only 3–8 % exhibited positive immunoreaction for an early transcription factor Pax2 specific to GABAergic and glycinergic inhibitory neurons suggesting that the majority of interneurons in DCM and LSCC projecting directly to the EUS motoneurons are excitatory.

Introduction

Storage and release of urine are dependent on the coordinated activity of the urinary bladder (BL) and the external urethral sphincter (EUS) muscles (Fowler et al., 2008). During urine storage the EUS is tonically active, while the BL is relaxed to promote continence. During micturition when the BL contracts the EUS relaxes in most species but in rats and mice the EUS exhibits alternating periods of relaxation and contraction which are thought to generate pumping activity that facilitates voiding (Kadekawa et al., 2016; Yoshiyama et al., 2000). EUS electromyographic (EMG) recordings during micturition in rodents exhibit bursting activity at frequencies of $4-5$ Hz consisting of silent periods approximately 100 ms in duration and active periods approximately 70 ms in duration (Cheng et al., 1997; Cheng and de Groat,

2010; de Groat et al., 1998; Kruse et al., 1993). Block of EUS bursting with alpha bungarotoxin reduces voiding efficiency (Yoshiyama et al., 2000).

In rats with an intact neuraxis bladder contractions and EUS bursting are initiated by a long latency spinobulbospinal pathway induced by Aδ bladder afferent input that activates circuitry in the pontine micturition center (de Groat et al., 1998); while tonic EUS activity is activated by a short latency spinal pathway organized in the L6-S1 spinal cord (Chang et al., 2007). After thoracic spinal cord transection in rats the EUS bursting is initially lost but returns several weeks after spinal transection in association with the emergence of automatic micturition. However the bursting reflex occurs with a shorter central delay and is dependent upon neural circuitry in the L3-L4 spinal cord (Chang et al., 2007). Transection of the cord caudal to L4 eliminates

EUS bursting but preserves tonic EUS activity and reflex bladder contractions. Thus, it has been proposed that neurons in L3-L4 have bi-directional communication with circuitry in the L6-S1 spinal segments to receive afferent signals from the bladder and in turn send efferent signals back to EUS motoneurons and/or interneurons in the L6-S1 spinal cord to generate EUS bursting. This second spinal component of lower urinary tract control in L3-L4 has been termed the lumbar spinal coordinating center (LSCC) because it appears to be essential for the coordination of BL and EUS activity during micturition.

In the present study we used pseudorabies virus (PRV) transsynaptic tracing techniques to identify the spinal interneurons (INs) in the lumbosacral spinal cord involved in the coordination of EUS-BL activity. Previous studies have mapped the central circuitry controlling various pelvic organs including the bladder, EUS, colon, kidney, urethra, penis (Barbe et al., 2018; Nadelhaft and Vera, 1996; Nadelhaft et al., 1992; Qin et al., 2007a; 2007b; Schramm et al., 1993; Vizzard et al., 1995) as well as the bulbocavernosus muscles (BCM) mediating ejaculation (Dobberfuhl et al., 2014; Truitt and Coolen, 2002; Xu et al., 2006). The latter muscles like the EUS exhibit bursting activity that is mediated by circuitry in the L3-L4 spinal cord; and PRV tracing from the BCM has identified neurons in L3-L4 that are essential for the BCM bursting activity (Marson and McKenna, 1996; Truitt and Coolen, 2002). However, it is unknown whether EUS and BCM share some portions of their spinal circuits.

To identify labeled neurons in the spinal cord we used PRV expressing reporter genes that produce green or red fluorescent proteins (GFP or RFP, respectively). After infection of peripheral organs the expression of a tracer in spinal neurons occurs many hours later due to the time necessary for retrograde transport of the virus along the peripheral axons to the spinal cord and infection/expression in efferent neurons (i.e., EUS motoneurons and bladder preganglionic neurons) followed by transsynaptic transport, expression and accumulation of the reporter in first order interneurons synaptically linked with the efferent neurons. Typically there is a 24 h delay between infection of a peripheral organ and the detection of label in the efferent spinal neurons that send axons to the peripheral organs and an additional $6 - 12$ h delay for labeling adjacent synaptically linked neurons in a local spinal network (Banfield et al., 2003; Gao et al., 2014; Jansen et al., 1995; Nadelhaft et al., 2002; Sugaya et al., 1997). Therefore, the delay in sequential transport between different neurons in a circuit makes it theoretically possible to identify the synaptic linkage in a circuit, i.e., discriminate second order interneurons from first order interneurons that directly synapse with the efferent motoneurons either by a large difference in expression time (for pairs of distant neurons) or based on differences in the intensity of fluorescence (for neurons of a compact local network). The latter implies that at certain post-infection times neurons infected earlier will exhibit a higher intensity of fluorescence than those infected later via synaptic connections provided other factors influencing PRV expression have lesser impact.

Using the PRV tracing technique we have identified EUS-related and BL-related INs in both L6/S1 and L3/L4 segments confirming existence of the hypothesized second compartment (LSCC) of the spinal LUT circuit. In the transverse sections of L6/S1 and L3/L4 fluorescently labeled interneurons were found exclusively in the central canal area (lamina X and inner lamina VII). No labeled cells at the time of counting were found in dorsal or ventral laminae or in the IML. Variation in the level of PRV expression has also provided some insight into the organization of the LSCC. Intimate interactions of EUS and BL spinal networks were also revealed by the co-expression of both reporters in some PRV-labeled cells and by the variation in the level of expression of each reporter in different cells. Immunostaining for Pax2 an early transcriptional factor specific to GABAergic and glycinergic neurons revealed that a minority of PRV-labeled EUS-INs were inhibitory neurons.

Experimental procedures

In this study we used male Sprague-Dawley rats at the age of P30-P35. Rats were kept in the animal facilities under a 12-h light-dark cycle with water and food *ad libitum*. To label EUS-related spinal circuitry with PRV, rats were anesthetized with isoflurane; the EUS was exposed by a longitudinal abdominal incision and the rostral part of the pubic bone was partially removed. Using a Nanoliter 2010 micro-injector (WPI, Sarasota, FL) PRV512 (or PRV-GFP) encoding EGFP (Bartha strain; titer 1.3×10^9 pfu/mL) was injected into the EUS striated muscles of the ventro-lateral walls of the middle third of urethra at 5–6 sites on each side (2.5–3 µL total). For identification of BL-related INs in the same animal we injected a total of ~ 5–6 µL of PRV614 (or PRV-RFP) encoding RFP (Bartha strain; titer 1.3×10^9 pfu/mL) into the BL wall at $\sim 10 - 12$ sites around the base of the BL. Viral tracers PRV512 and PRV614 were obtained from Dr. L.W. Enquist (Virus Center grant # P40RR018604). These dual injections allowed labeling of neurons in both circuits. At each injection site the needle was left in place for $1 - 2$ min to avoid virus leakage. To control possible leakage a small amount of Fast Green FCF 0.5 % (Electron Microscopy Sciences, Hatfield, PA) was added to the viral solution, so that any fluid coming back would be immediately visualized. In none of the cases did the virus leak back.

PRV labelling in the spinal cord was not optimal on the 2nd day after PRV injection into the EUS when only EUS-MNs in Onuf's nucleus exhibited fluorescence ranging from bright to moderate, but interneurons in the dorsal commissure (DCM) and LSCC were not labeled. The best labeling of EUS-related interneurons in the L6/S1 DCM and L3/L4 LSCC was observed on the 3rd post-inoculation day. Therefore, on the 3rd day after PRV injection rats were perfused with 4% paraformaldehyde, spinal cords were removed, cut into two sections containing the S2-L5 and L4-L1 segments and put into the fixative. After infiltration with 25 % sucrose the spinal cords were cut on a cryostat to 50 µm thick sections and placed sequentially on slides. Hence, mapping of labeled cells throughout all transverse sections in the order of cutting would provide a 3D representation of their distribution in the spinal cord. Quantitative data in this paper were obtained from three animals.

In order to detect locations of interneurons involved in (a) the EUS-related and (b) the BL-related networks we combined tracing from both EUS and BL. However a problem with dual tracing experiments was that the BL circuit, unlike the EUS circuit, includes an extraspinal synaptic junction in the major pelvic ganglion, which would add a time lag in the transport of PRV to BL preganglionic neurons in the spinal cord and in turn add a delay in transsynaptic transport and expression in BL-related interneurons compared to labeling of EUS-related interneurons (EUS-INs). Therefore, when equal amounts of PRV-512 (green) and PRV-614 (red) were injected simultaneously into the EUS and the BL wall in preliminary experiments, green staining was detected in EUS-INs at the selected optimal post-inoculation time (3 days) but red staining in BL-related interneurons (BL-INs) was scarce or absent. This indicated that at the time of perfusion PRV-614 was not optimally expressed in BL-INs due to the additional peripheral time lag. Dual PRV tracing experiments conducted by other investigators (Cano et al., 2004) revealed that when PRV strains with different levels of invasiveness were injected into different organs the weak labelling by one strain could be improved by injecting larger volumes of that strain. Other authors also show positive correlation of virus titer or applied volume with the magnitude of viral proliferation and expression of the reporter (Card et al., 1995; Guo et al., 2017; Hillyer et al., 2018; Metts et al., 2006).Thus, to overcome the problem of unequal labelling in our preliminary experiments and to equalize fluorescence intensities in labeled EUS-INs and BL-INs, we tested the method of Cano et al. (2004) to determine if it could eliminate the difference in timing of PRV labelling in EUS and BL related circuits. When the volume of PRV injected into the BL wall was $\sim 1.5 - 2$ times larger than the volume injected into the EUS both populations of interneurons demonstrated a similar time course and

DCM

LSCC

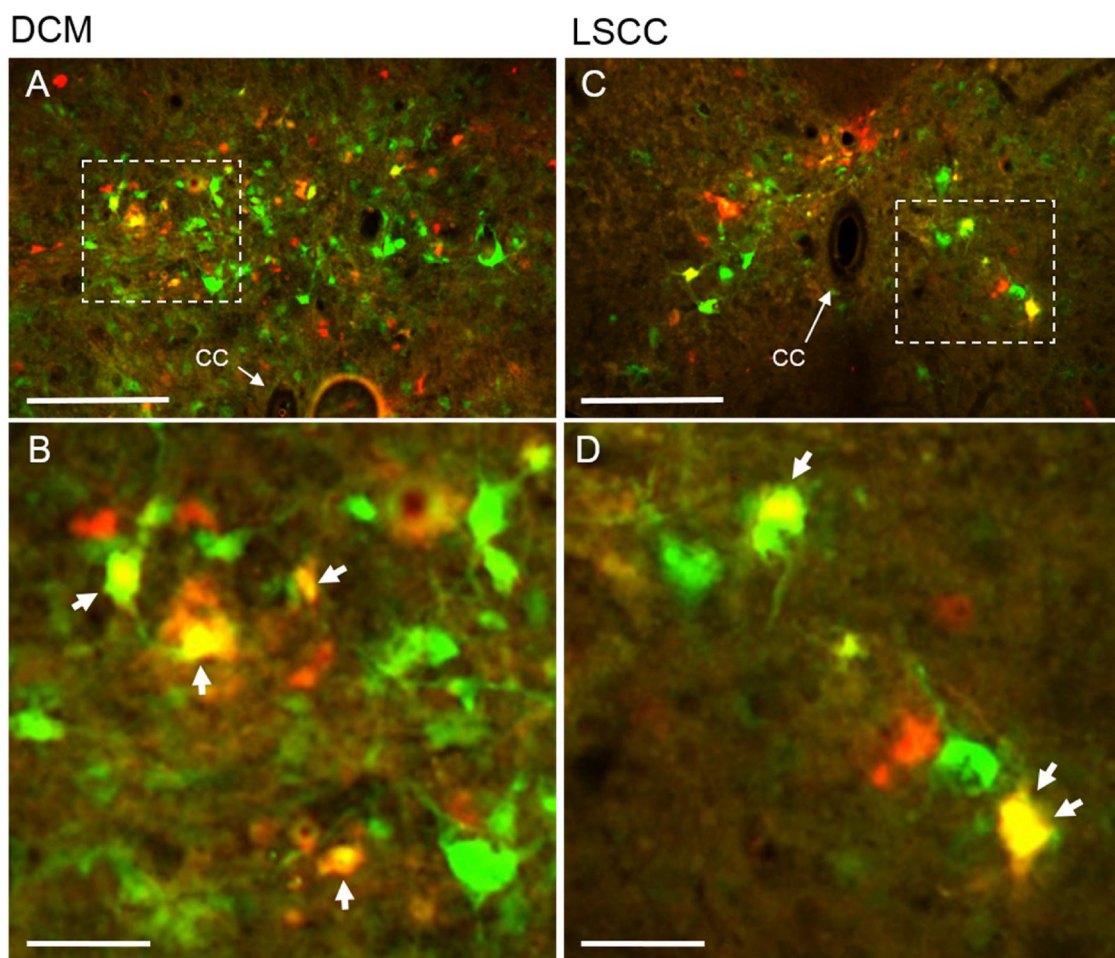**Fig. 1.** Concomitant labeling of EUS-related (GFP, green) and BL-related (RFP, red) interneurons in the L6/S1 DCM (*A, B*) and L3/L4 LSCC (*C, D*) in single 50 μm thick sections. Colocalization of the two markers in the same cell results in yellow staining (indicated by arrows in *B, D*) with variable proportions of green and red components in different cells. Lower rows show magnified images in the squares above. Scale bars in *A, C* are 200 μm and in *B, D* are 50 μm (For interpretation of the references to colour in this figure legend, the reader is referred to the web version of this article.).

intensity of staining. This can be explained by dependency of PRV transport and expression not only on time, but also on the number or concentration of infecting viral particles. Using this method output neurons related exclusively to the EUS circuit (i.e., EUS motoneurons) were labeled only by green fluorescence, and output neurons related exclusively to the BL circuit (i.e., sacral parasympathetic preganglionic neurons, SPPNs) were labeled only by red fluorescence. The majority of interneurons were either green or red, whereas some interneurons that were presumably involved in both circuits and infected simultaneously by both virusesexpressed both markers and had yellow staining after superposition of green and red images (Fig. 1).

Fluorescent images of each section were obtained on a Leica DM5000B microscope equipped with LAS-X software. Excitation filters were BP 470/40 for GFP and BP 525/50 for RFP; suppression filters were BP 546/12 for GFP and BP605/75 for RFP. To obtain a uniform set of images the intensity of background auto-fluorescence was taken as a reference intensity and in all sections of a given spinal cord fragment it was constant. To register all of the labeled cells and at the same time discriminate cells by fluorescent intensities we used long and short exposures when imaging each section. First, an image of a section was photographed with a relatively long exposure so that all labeled cells were visible on the background of auto-fluorescent gray matter, but in this case the majority of cells emitted light exceeding the camera saturation level and were indistinguishable by their brightness. The second snapshot of the same image with a short exposure resulted in visualization of only the brightest neurons while moderately/poorly

fluorescent neurons were hardly visible or totally invisible in the dark background (Fig. 2, pairs A,D and G,J). These pairs of selected exposures were kept constant when examining all sections of a given fragment of the spinal cord. This approach allowed discrimination of the brightest neurons (bright red, B_R, or bright green, B_G) with full expression of a fluorophore from those with weaker incomplete expression (weak red, W_R, or weak green, W_G). As an alternative approach for discrimination of brightly labeled cells from moderately or weakly labeled cells we used 3D and 2D color histograms (maps) built over an image. In 3D color maps Z-peaks of various amplitudes corresponded to pixel intensities on an XY-image (Fig. 2 C, F, I, L). For short-exposure images a few peaks usually created a cluster with close to near-saturating amplitudes which were significantly higher than a set of lower peaks with an indiscriminative continuum of amplitudes. This allowed for separation of a cluster of these highest peaks (i.e. the brightest cells) from a set of lower peaks corresponding to moderately/ weakly fluorescent cells. There was no further attempt to separate distinctive groups among lower amplitude peaks. In general, the "two-exposures" approach and 3D-histogram approach gave the same results for discriminating the brightest cells from moderately or weakly labeled cells. With a threshold set at 5% of the full scale the conversion of the 3D to the 2D color map resulted in the same patterns of "thresholded" neurons as the patterns of the brightest cells in an original image (Fig. 2 B, E, H, K). As an additional approach the thresholding routine in Neurolucida 11 software package was tested and generated similar results. For generation of quantitative data we used the "two-exposures"
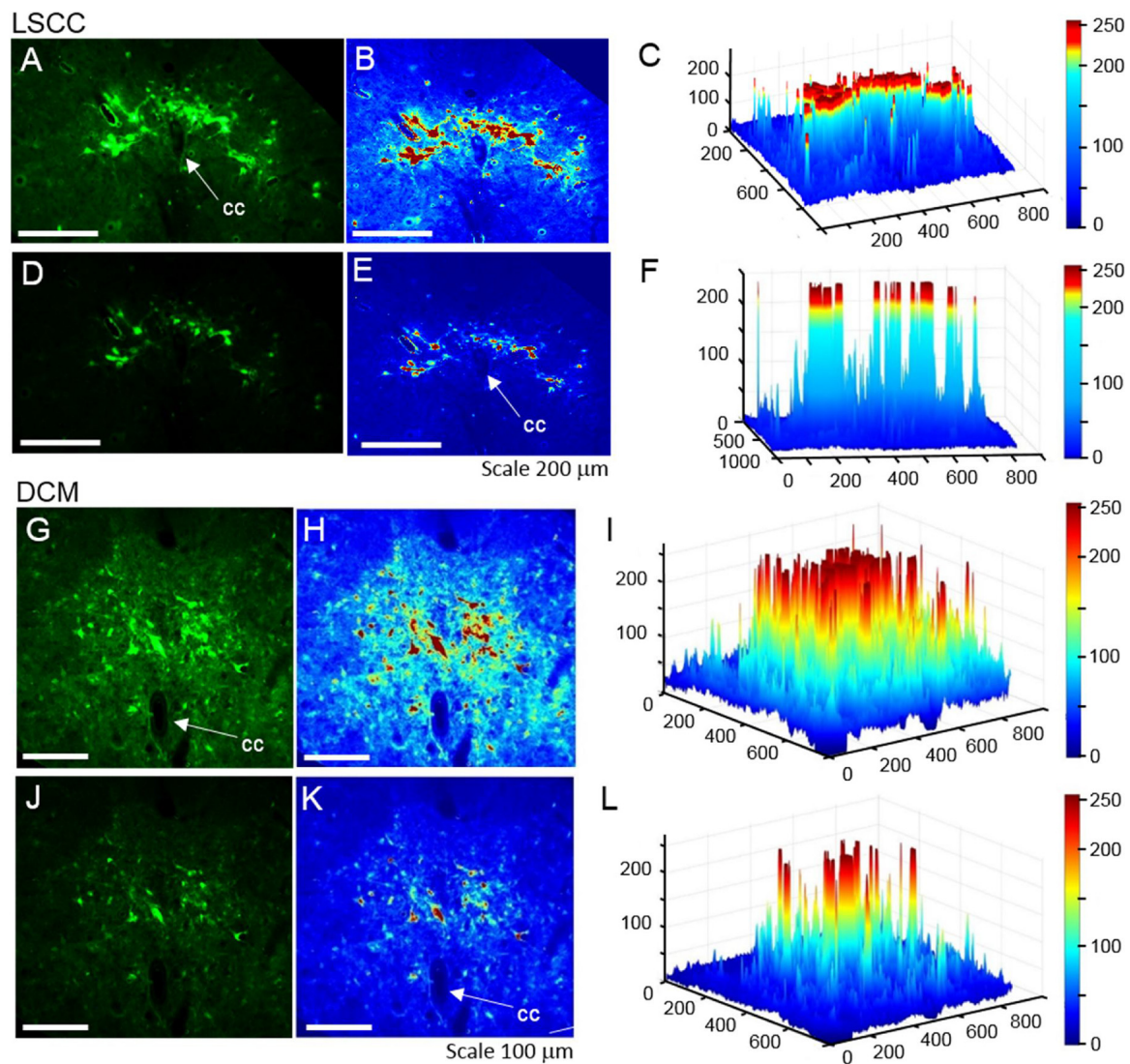
Fig. 2. Trans-neuronal labeling of spinal interneurons with PRV512 encoding EGFP injected into the EUS and discrimination of infected neurons by brightness of GFP fluorescence. Panels A—F contain information about a single section through the LSCC in the L3 spinal segment and panels G-L contain information about a single section through the DCM in the L6 spinal segment. *A* and *G*, long exposure photomicrographs of 50 μm thick sections reveal all GFP positive neurons in the LSCC and DCM, respectively. *D* and *J*, short exposure photomicrographs of the same sections adjusted to obtain a signal of a slightly sub-saturation level of camera sensitivity revealing only the brightest neurons in the LSCC and DCM. Fluorescence intensities of the LSCC section in panels *A* and *D* are depicted in 2D (*B and E*, respectively) and 3D (*C and F*, respectively) color maps. The dark-red/brown stain in the color maps designate the upper 5% of the scale range (the scale is in relative units). In the 3D-map for a short exposure (*F*) positions of peaks with brown tops correspond to brown-stained cells in the 2D-map (*E*) and to positions of the brightest cells in *D*. These peaks can be discriminated as a group from a continuum of lower peaks (yellow and green in color maps), thus showing reliability of all three methods for discrimination of the brightest cells. Similarly, fluorescence intensities of the DCM section shown in panel *G* at long exposure and in panel *J* at short exposure are depicted in 2D (*H and K*, respectively) and 3D (*I and L*, respectively) color maps. Positions of brown-stained peaks in *L* correspond to positions of brown-marked cells in *K* and positions of the brightest cells in *J*. 3D-maps in *F* and *L* clearly demonstrate a multitude of moderately or weakly fluorescent neurons (yellow and green in color maps) significantly less bright as compared to brown-marked cells. Note, that all images and color maps in *A-F* were obtained from a single 50 μm section of LSCC; similarly, images and color maps in *G-L* were obtained from a single 50 μm section of DCM. In 3D color maps (*C, F, I, L*) X and Y axes are in pixels and Z axis is in relative units. The central canal (CC) is indicated by an arrow. Scale bars are 200 μm in *A, B, D, E* and 100 μm in *G, H, J, K* (For interpretation of the references to colour in this figure legend, the reader is referred to the web version of this article.).

method.

All labeled interneurons were separated by color and brightness of staining, mapped and counted in sequential transverse sections. Because of the potential of "double counting" of the same cell in adjacent sections several approaches were used to avoid this possibility. First, only cell-shaped units usually with proximal parts of dendrites were counted and all other fluorescent elements (pieces of dendrites, synaptic boutons, debris of destroyed neurons) were discarded. Second, elements of the size less than 5 μm (usually weakly stained) which could represent a part of a cut cell were not counted as we defined it as a minimal size of biocytin-filled and reconstructed EUS-INs (Karnup

and de Groat, 2020). Third, by overlapping adjacent maps we checked for coinciding dots which would indicate potential double-count; such precise overlap of dots was very rare, but when it happened one of the dots was removed. However, despite these precautions there is no guarantee that some cells might be counted twice. Thus, the total number of labeled cells may be somewhat overestimated. Before neurons were mapped and counted, images of all sections were centered on the central canal (CC) and rotated (and flipped if necessary) using homemade MATLAB script to unify their orientation and recover the original structure of the spinal cord. Mapping and counting of labeled neurons was performed using Neurolucida-11 software. To visualize co-
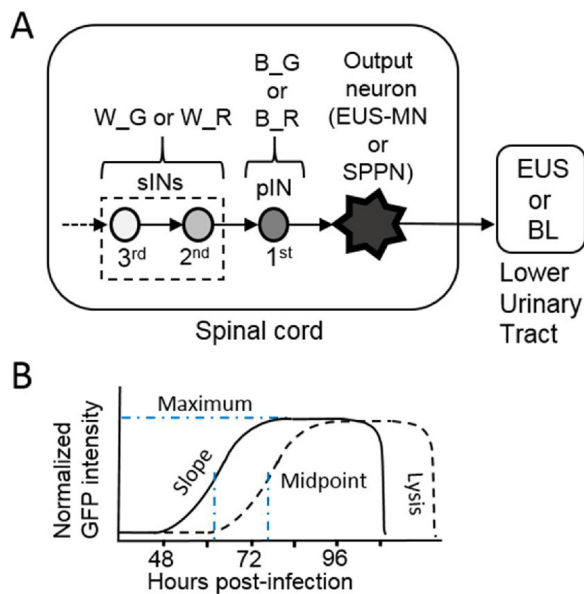
Fig. 3. A - Correspondence between intensity of fluorescence in PRV-labeled interneurons and their presumed order in a circuit. B_G – bright green, B_R – bright red, W_G – moderately or weakly green, W_R – moderately or weakly red; pIN – primary interneuron presynaptic to an output neuron, sINs – secondary interneurons of higher orders modulating activity of pINs, EUS-MN –motoneuron of the external urethral sphincter, SPPN– sacral parasympathetic preganglionic neuron in the bladder circuit. The order of an interneuron in the spinal network is indicated below the cell symbol. B – Hypothetical model of sequential PRV infection of two synaptically connected cells (postsynaptic, solid line; presynaptic, dashed line) based on accumulation of a reporter protein (GFP) in single cells (from Fig. 2E in (Guo, et al., 2017)), the minimal time lag between reporter accumulation in post- and presynaptic cells and the average PRV proliferation rate (our observations and those of (Bienkowski, et al., 2013;Cano, et al., 2001;Jovanovic, et al., 2010;Kim, et al., 2000;Lee and Erskine, 2000;Metts, et al., 2006;Taylor et al., 2012)). Cumulative distribution function illustrates a ≥ 12 h delay between PRV infections in a postsynaptic and a presynaptic neuron. Virus proliferation and GFP accumulation to maximum level require ~ 12 h, and first bright pINs appear on day 3 (72 h). Hence, the maximal GFP brightness in a pIN at a time when intensity of fluorescence in a presynaptic sIN is around half-maximal. However, on day 4 (96 h) both pINs and sINs should be brightly labeled and, therefore, indistinguishable (For interpretation of the references to colour in this figure legend, the reader is referred to the web version of this article.).

expression of GFP and RFP the green and red images of each section were merged using ImageJ software.

As expected, brightness of fluorescence in labeled cells was not uniform. Typically, a few neurons in a section were brightly labeled while others were noticeably less bright or weakly labeled but more numerous. Due to time lags necessary for retrograde transport of PRV throughout the spinal networks it seems reasonable to expect that interneurons synaptically connected to the efferent/output neurons and infected earlier (termed in this study first order or primary interneurons, pINs) would exhibit higher intensity of fluorescence than the fluorescence of interneurons presynaptic to the pINs (termed second order or secondary interneurons, sINs) that would be infected later (Fig. 3A). Thus, in our analysis bright red (B_R) or bright green (B_G) interneurons were classified as pINs and weak red (W_R) or weak green (W_G) were classified as sINs (Fig. 3A). In most studies with transneuronal PRV tracing the expression of the reporter protein in a presynaptic cell has ~ 12 h-24 h delay as compared to that in a post-synaptic cell (Bienkowski et al., 2013; Cano et al., 2001; Jovanovic et al., 2010; Kim et al., 2000; Lee and Erskine, 2000; Metts et al., 2006). Since in our experiments first weakly labeled INs could appear on day 2, but bright INs were seen only on day 3, we conclude that the labelling occurred in the same cells and that one additional day was necessary for

reporter expression to reach the maximum brightness. Assuming that infection of a sIN starts at ≥ 12 h after a pIN is infected, the maximum brightness in a pIN will be reached when GFP accumulation in sIN has started but not reached its maximum (Fig. 3B). In other words, during the next 12 h time period weakly or moderately bright neurons can be discriminated from brightly fluorescent cells and with high probability can be considered the next order neurons in the circuit.

To identify neurons with colocalization of two markers, images of the same cell at each emission wavelength were classified as bright or weak and merged to obtain a combined color. The latter technique yielded four combinations: a) bright yellow labeling if labeling by green and red was similarly bright (B_G + B_R), b) weak or moderate yellow labeling if labeling by green and red was similarly weak (W_G + W_R), c) greenish yellow if green staining prevailed (B_G + W_R), and d) reddish yellow if red staining prevailed (B_R + W_G). Thus, B_G + B_R cells are considered to be pINs and presynaptic to output neurons of both the EUS and BL; W_G + W_R cells are considered to be sINs involved in both circuits; B_G + W_R cells are considered to be pINs in the EUS circuit (EUS-pIN) and at the same time sINs in the BL circuit (BL-sIN); B_R + W_G cells are considered to be involved as pINs in the BL circuit and as sINs in the EUS circuit. However this interpretation might be influenced by several other factors that potentially influence the time necessary for full expression of reporters. For instance, the rate of PRV transition from a post-synaptic to a presynaptic neuron depends on availability and number of specific receptors necessary for PRV to invade the presynaptic cell and on the number of synaptic contacts between two cells. Thickness of an axon, rate of axonal transport, size of a cell and variations in DNA transcription rate could also play a role. Concentration of viral particles at the site of injection may also influence the virus uptake and transport rate as shown in preliminary experiments for PRV injected to the BL wall. Although these factors may make a minor contribution to the different levels of fluorescence, the stepwise variation in brightness between cells (see data in the results section) suggests that the different levels reflect the position of the cells (Fig. 3) in the EUS and BL spinal networks.

In a separate series of experiments (3 rats) designed to determine the location of a descending propriospinal pathway connecting LSCC and EUS-MNs, we made dual injections of different viral tracers: (1) antero-retrograde viral tracer AAV-ChR2-GFP (Penn Vector Core) (6–8 points, 900–1000 nl total, titer 10^{13}GC/mL) injected unilaterally into the L3/L4 segments near the central canal to reveal the course of descending axons, and (2) PRV into the EUS as described above to label EUS-MNs. The injection of AAV-ChR2-GFP was performed under isoflurane anesthesia via a laminectomy of the first lumbar vertebra and with a micropipette inserted obliquely (~ 30°) to a depth of ~ 700 μm from the dorsal surface of the spinal cord. The location of the injection site in the L3/L4 segments was later verified histologically. Four weeks after the injection of AAV-ChR2-GFP into the spinal cord abdominal surgery was performed to inject PRV614 into the EUS. The spinal cord was removed 3 days later and processed as described above. Thus, in histological section of the spinal cord we expected to see EUS-MNs in L6/S1 exhibiting red fluorescence due to PRV614 labelling and axonal arborizations from L3/L4 interneurons labeled with green fluorescence projecting to EUS-MNs or interneurons in L6/S1.

To identify inhibitory cells among EUS-INs we used Rabbit-anti-Pax2 primary antibody (1:1000) and Donkey-anti-Rabbit-Alexa-Fluor-488 secondary antibody (1:500) (Abcam, Cambridge, MA). Pax2 is an early transcription factor which is expressed in GABA-ergic and glycinergic inhibitory neurons (Huang et al., 2008; Batista and Lewis, 2008). In adult animals it is present in nuclei of inhibitory cells (Larsson, 2017). In these experiments the EUS was injected with PRV-614 (PRV-RFP). Therefore, in double-stained Pax2-positive neurons nuclei were always yellow.

Data analysis was performed using Origin8 (OriginLab Corporation,Northampton, MA), SigmaPlot12 (Systat Software, Inc., San Jose, CA) and MATLAB 7.10 (MathWorks Inc., Natick, MA)
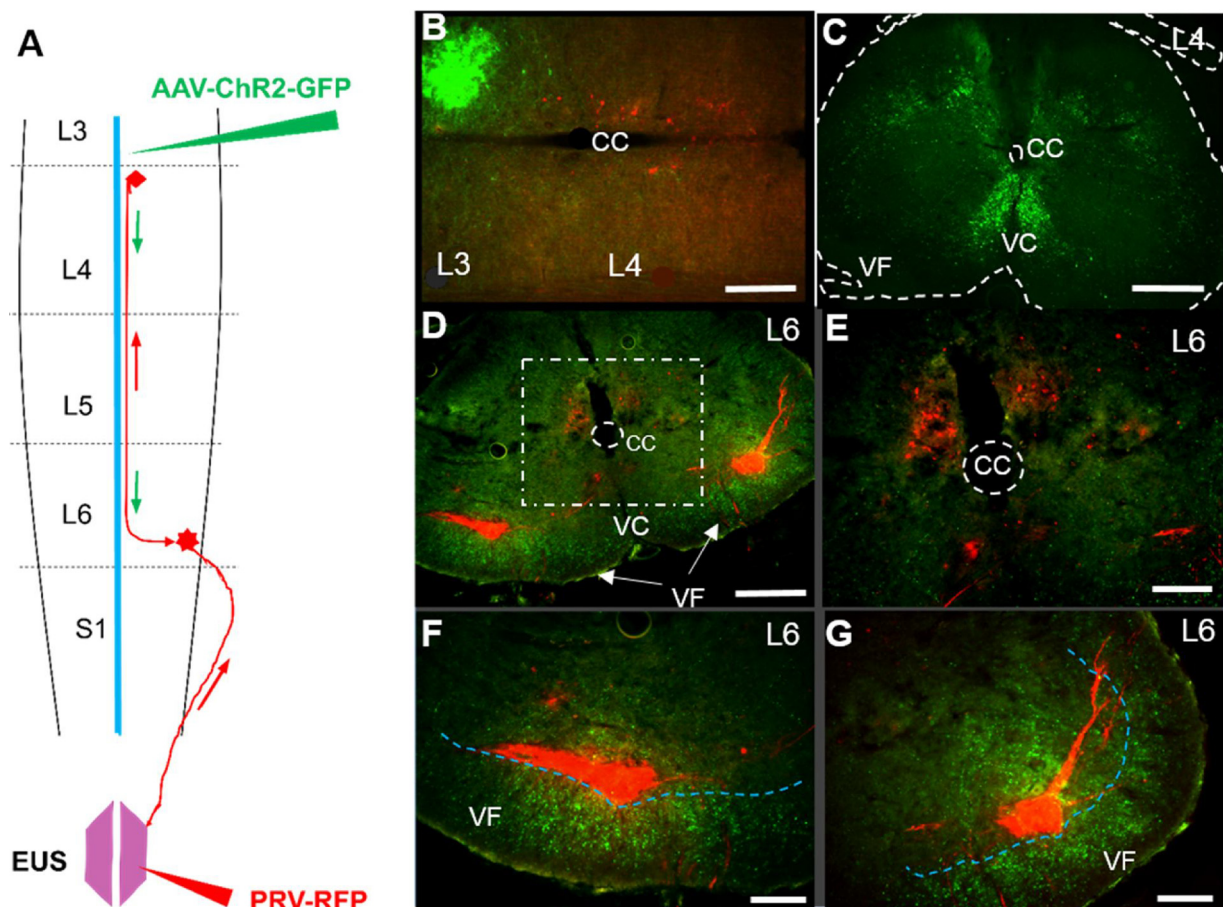
Fig. 4. Axonal projections from L3/L4 LSCC to L6/S1. **A** - Diagram of AAV-ChR2-GFP injection in L3/L4 near the central canal (CC) and PRV-RFP injection in the EUS. Green arrows indicate direction of anterograde propagation of AAV-ChR2-GFP. Red arrows indicate retrograde trans-synaptic propagation of PRV-RFP in the EUS-related circuit. **B** – In a horizontal section of the spinal cord a limited area of AAV-ChR2-GFP injection in lamina X and inner lamina VII of L3 is visible as a green spot. There are a few LSCC neurons in L4 traced with PRV-RFP from the EUS. **C** – In a transverse section axons anterogradely traced with AAV-GFP in the caudal end of L4 descend within the ventral column (VC). **D** – In L6 transverse section labeled axons descending from L3/L4 ramify in the ventral funiculus (VF) and densely arborize in the ventral horn around Onuf's nucleus. **E** – Zoomed area of the dashed square from D. Axonal arborization in the DCM and around CC is sparse. Local EUS-related interneurons labeled with RFP are located in the DCM above the CC. **F and G** – magnified clusters of EUS-MNs (left and right correspondingly) shown in D are surrounded with a profound GFP-labeled axonal arbor. In B-D scales are 500 μm, in E-G scales are 200 μm (For interpretation of the references to colour in this figure legend, the reader is referred to the web version of this article.).

software packages. Data are presented as mean ± SD or mean ± SE and differences were assessed for significance with the Welch *t*-test. For mapping and counting of fluorophore-filled cells we used Neurolucida11 (MicroBrightField, Colchester, VT) and ImageJ (NIH, Bethesda, MD). Figure preparation was done with the CorelDraw12 (Corel Corporation, Ottawa ON, Canada) and PowerPoint (Microsoft Corporation, Redmond, WA) software. All chemicals were purchased from Sigma (St. Louis, MO).

Results

Descending projections from L3/L4 to L6/S1

For the first time we identified location of the descending axonal pathway connecting L3/L4 and L6/S1 neuronal circuits. Axons of L3/L4 propriospinal neurons connecting LSCC with EUS-MNs and other neurons in L6/S1 were revealed with the anterograde viral tracer AAV-ChR2-GFP (Fig. 4 A). After injection of AAV-ChR2-GFP near the CC in L3/L4 fluorescent fibers were identified in the ventral column (in L4/L5) and in the ventral funiculus (in L6/S1) (Fig. 4 B). Although stained axons could obviously belong to different systems, the pathway connecting LSCC and EUS-MNs and/or other neurons in L6/S1 segments should also be located within the ventral column. In L6/S1 GFP-labeled

axonal arborizations were found mostly in the ventral horn around Onuf's nucleus, indicating that LSCC propriospinal neurons indeed can be presynaptic to EUS-MNs and probably to other surrounding cells {Fig. 4 C–G}. Thus, this finding confirms the previously suggested location of the LSCC-to-L6/S1 descending pathway within ventral column and ventral funiculus (Karnup and de Groat, 2020).

Distribution of EUS and bladder interneurons

The general distribution of labeled interneurons was similar for the bladder and EUS circuits if only one organ was injected with PRV or if the EUS was injected with PRV-512 (green) and the bladder was injected with PRV-614 (red). In transverse sections of L6/S1 and L3/L4 the population of interneurons traced from EUS (EUS-INs) and population of interneurons traced from BL (BL-INs) were overlapping. In L6/S1 EUS-INs were located in the DCM dorsal to the central canal (CC) (Fig. 5, green), and in L3/L4 they were scattered dorsal and lateral to the CC (Fig. 6, green). BL-INs in L6/S1 (Fig. 5, red) and in L3/L4 (Fig. 6, red) segments occupied the same intraspinal space near the CC, but their area of distribution in transverse plane was wider than that for EUS-INs, reaching $1/3 - 1/2$ of the distance between the CC and the lateral funiculus (Lf) (Figs. 5A and 6A, red).
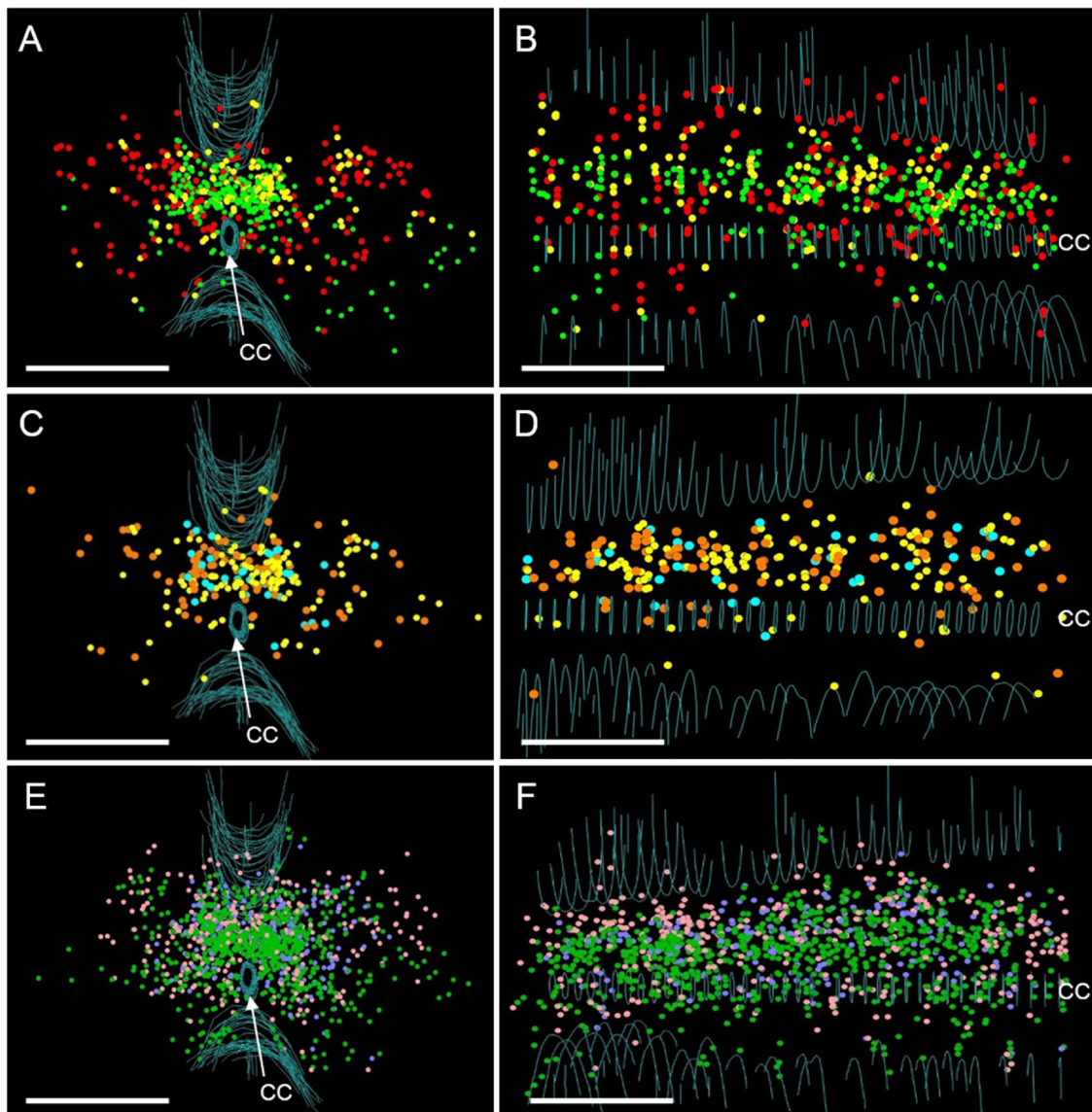
Fig. 5. Maps of INs in L6/S1 DCM traced from the EUS with PRV512 (GFP) and traced from the BL with PRV614 (RFP) in the same animal. Left column – transverse view of the composite created by superimposing the maps of 40 sequential sections. Right column – lateral view on sets of corresponding maps after rotation to 90°, caudal side is on the left. *A, B* – Brightly fluorescent interneurons were considered neurons of the 1st order presynaptic to output neurons. They were divided into three groups: (1) B_G – bright green fluorescence corresponding to EUS-related spinal neurons presynaptic to EUS-MNs, (2) B_R – bright red fluorescence corresponding to BL-related neurons presynaptic to BL-SPPNs and (3) bright yellow neurons that simultaneously showed bright green and bright red fluorescence. *C, D* – Neurons in these maps are immediately presynaptic to at least one kind of output neurons: (1) B_G + B_R neurons (yellow dots) are equally involved in both circuits; (2) B_R + W_G (orange dots) designate neurons with predominating bright RFP staining and weaker GFP staining; (3) B_G + W_R neurons (blue dots) designate neurons with predominating bright GFP staining and weaker RFP staining. *E, F* – Interneurons with moderate or weak staining are considered to be 2nd order cells and are divided into three other groups: (1) W_G – weak or moderate green fluorescence (dark green dots), (2) W_R – weak or moderate red fluorescence (pink dots), (3) W_G + W_R – superimposition of weak green and red fluorescence in the same cell (purple dots). Scale bars are 500 μm. Blue lines designate outlines of the CC, VMf and DMf in section (For interpretation of the references to colour in this figure legend, the reader is referred to the web version of this article.).

Identification of subpopulations of interneurons

All labeled interneurons were separated by color and brightness of staining (see below), mapped and counted in sequential transverse sections in three P30-P35 rats (Table 1). As expected, brightness of fluorescence in labeled cells was not uniform. Typically, a few neurons in a section within ~200 μm from the CC were brightly labeled (Figs. 5A,B, 6A,B and Table 2). Neurons exhibiting GFP and RFP colocalization where both markers were equally bright or where one marker was brighter than the other were generally distributed in the same area (Figs. 5 C, D and 6C, D). Weakly fluorescent cells were also widely scattered around CC (Figs. 5 E,F and 6E,F). As described in the Methods section we hypothesize that the interneurons with the brightest fluorescence are 1st order or primary interneurons (pINs), that are presynaptic to output neurons and infected early; whereas neurons presynaptic to the pINs, i.e., 2nd or 3rd order interneurons (sINs) are infected later and express weaker fluorescence. However, several other factors might influence the time necessary for full expression of reporters (see list of factors in the Methods section). Each of these factors could lead to variable brightness of cells of the same order. However, all of these factors should have effects that are normally distributed. Hence, if their combined impact had a predominating effect on the apparent/estimated cellular order in a neural circuit, then there should be a continuous range of brightness among labeled neurons rather than a quantal or stepwise variation in brightness between cells. In our experiments the images obtained with different exposures and assessed
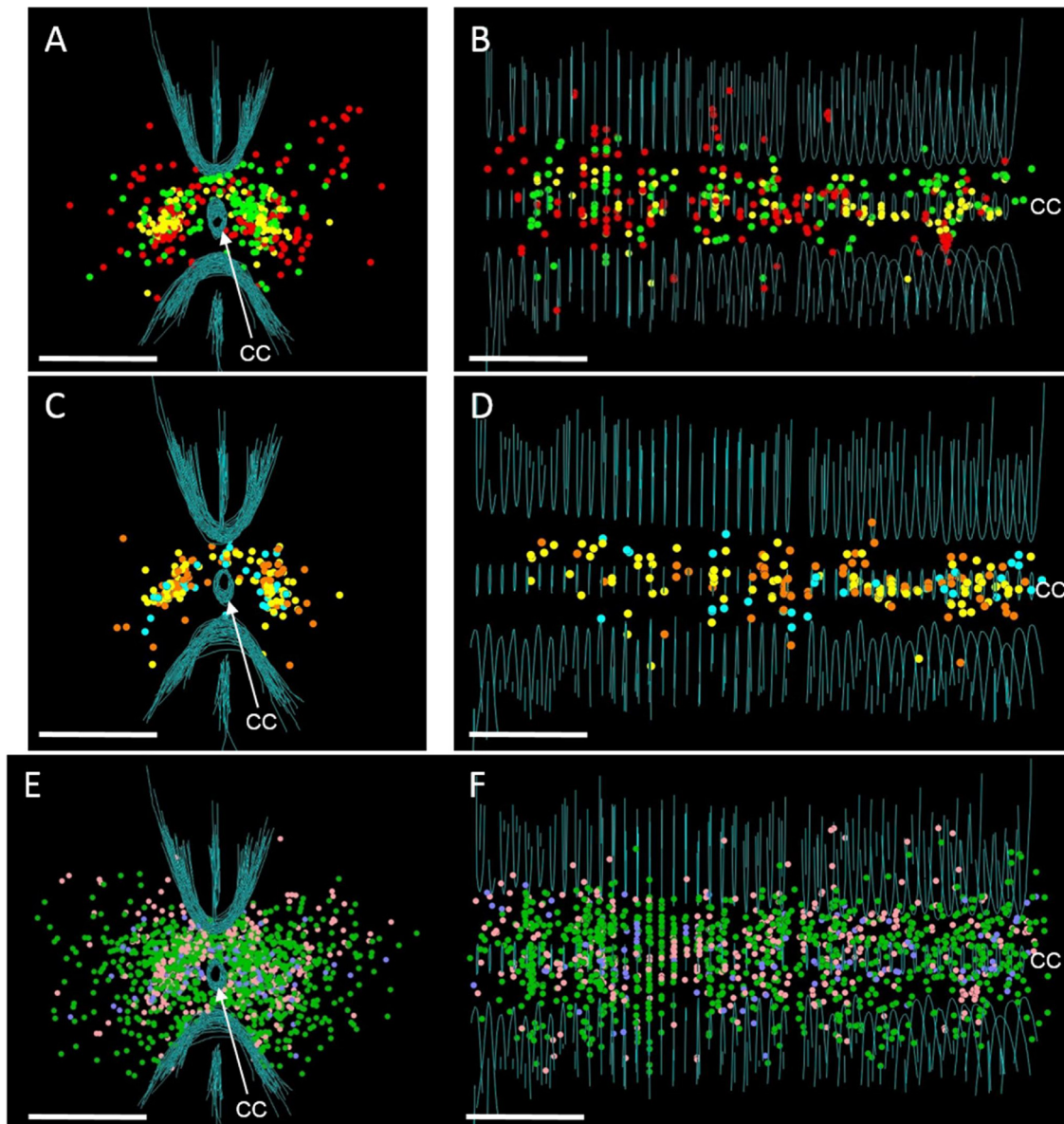
Fig. 6. Maps constructed over 46 sequential sections of L3/L4 of one animal. Interneurons traced in LSCC from the EUS with PRV512 (GFP) and from the BL with PRV614 (RFP) of the same spinal cord shown in Fig. 5. Left column – transverse view of superimposed maps. Right column – lateral view of sets of corresponding maps after rotation to 90˚, caudal side is on the left. All designations of cell types and color coding are the same as in Fig. 5. Scale bars are 500 μm. Blue lines designate outlines of the CC, VMf and DMf in section (For interpretation of the references to colour in this figure legend, the reader is referred to the web version of this article.).

with 3D plots of fluorescence intensities show that at the earliest time of full PRV expression, the brightness of fluorescence within a pool of interneurons is distributed in a stepwise fashion between the brightest and less bright neurons (Fig. 2). Thus, the brightest interneurons have a high probability of being 1st order interneurons, while 2nd and 3rd order cells are not separable and are merged into one group.

Comparison of the distributions of subpopulations of EUS and bladder interneurons

Mapping of cells from sequential sections generated 3D maps showing the spatial distribution of each cell type and allowed us to compare the distributions of two or more cell types. Viewed in the transverse plane it is clear that EUS-pINs in the L6/S1 DCM and in the L3/L4 LSCC are significantly more compact in the transverse plane than BL-pINs (Figs. 5A and 6 A). Difference in the distribution of EUS-sINs and BL-sINs in DCM is less pronounced than for pINs (Fig. 5 E, F), and

there is almost no difference in the scattering of EUS-sINs and BL-sINs in the LSCC (Fig. 6 E, F).

By counting brightly labeled neurons expressing only one of the markers we found that a 50 μm section of the DCM contains on average 6.0 EUS-pINs and 3.9 BL-pINs (Fig. 7, Table 2); while there is a considerably higher number of moderately or weakly labelled cells in the DCM (38.1 EUS-sINs and 6.9 BL-sINs per section). Thus, in DCM the ratio of EUS-related

secondary-to-primary INs is 38.1–6.0 = 6.3, whereas the ratio of BL-related secondary-to-primary INs is 6.9 to 3.9 = 1.8, indicating that the EUS sIN circuit in the DCM is larger and potentially more complex than the BL circuit. The LSCC in the lumbar compartment contains on average 5.0 EUS-pINs and 2.4 BL-pINs per section and contains 25 EUS-sINs and 5.5 BL-sINs per section. Thus, the EUS circuit in the LSCC also has a higher secondary-to-primary IN ratio (5) than that in the BL circuit (2.3).

Table 1
Cell count of spinal interneurons trans-synaptically labeled from EUS (by GFP) and BL (by RFP).

Circuit and order of interneurons	Colors	E30		E31		E32	
		DCM (L6-S1) N = 40 s	LSCC (L4-L3) N = 46 s	DCM (L6-S1) N = 23 s	LSCC (L4-L3) N = 70 s	DCM (L6-S1) N = 44 s	LSCC (L4-L3) N = 90 s
EUS-primary Ins EUS-1st or pEUS_INs	Bright Green (B_G)	283 (7.0/s)	125 (2.7/s)	95 (4.1/s)	453 (6.5/s)	301 (6.8/s)	519 (5.7/s)
BL-primary Ins BL-1st or pBL_INs	Bright Red (B_R)	180 (4.5/s)	162 (3.5/s)	41 (1.8/s)	65 (0.93/s)	235 (5.3/s)	269 (2.99/s)
Type1_INs: EUS-1st / BL-1st (pEUS/pBL_INs)	Bright Yellow (B_Y = B_G + B_R)	134 (3.35/s)	89 (1.9/s)	8 (0.35/s)	101 (1.44/s)	60 (1.36/s)	138 (1.51/s)
Type 2a_Ins EUS-1st / BL-2nd/3rd (pEUS/sBL_INs)	Bright Green + Weak Red (B_G + W_R)	33 (0.8/s)	30 (0.65/s)	5 (0.22/s)	80 (1.14/s)	23 (0.52/s)	56 (0.62/s)
Type 2b_INs BL-1st / EUS-2nd/3rd (pBL/sEUS_INs)	Bright Red + Weak Green (B_R + W_G)	93 (2.3/s)	64 (1.39/s)	10 (0.43/s)	55 (0.8/s)	63 (1.43/s)	88 (0.98/s)
Type3_INs: EUS-2nd/3rd / BL-2nd/3rd (sEUS/sBL_INs)	Weak Green + Weak Red (W_G + W_R)	207 (5.1/s)	128 (2.78/s)	64 (2.78/s)	145 (2.07/s)	278 (6.3/s)	292 (3.24/s)
EUS-2nd/3rd (sEUS_INs)	Weak Green (W_G)	785 (19.6/s)	891 (19.3/s)	874 (38.0/s)	1488 (21/s)	2495 (56.7/s)	3105 (34.5/s)
BL-2nd/3rd (sBL_INs)	Weak Red (W_R)	332 (8.3/s)	329 (7.1/s)	72 (3.1/s)	134 (1.9/s)	410 (9.3/s)	682 (7.6/s)

Cell count of labeled interneurons in three male rats. Order of an interneuron either in EUS or in BL circuits was determined by intensity of staining (see Methods). Green fluorescence (G) identified neurons of the EUS circuit, and red fluorescence (R) identified neurons of the BL circuit. Cells exhibiting both green and red fluorescence are considered to be involved simultaneously in EUS and BL circuits either as primary or secondary interneurons. First order or primary interneurons (pEUS_INs and pBL_INs) involved in the circuit of only one organ exhibited either bright green (B_G) or bright red (B_R) staining, whereas cells included in both circuits as primary interneurons (Type1) showed bright yellow (B_Y) staining in merged images. Moderately or weakly stained cells (W_G and W_R) are considered secondary interneurons (sEUS and sBL) of 2nd or 3rd orders. Types 2 and 3 cells represent dual labelling created by three combinations of primary and secondary neurons as indicated in the table. Cell count is presented as a total number of cells (without parenthesis) and as a number of cells per section (in parenthesis). N – number of sections. E30-E32 – identification numbers for three animals.

Convergence of EUS and bladder circuitry in the DCM and LSCC

In addition to purely green and purely red staining in superimposed images we observed yellow cells suggesting colocalization of the two markers (Fig. 1). The spectrum of yellow staining was not uniform and ranged from yellow to greenish-yellow or to reddish-yellow reflecting differences in the proportions of expressed markers among double-labeled cells. We presume that bright yellow staining results from equally bright green and red fluorescence (termed: B_G + B_R), indicating that these neurons are pINs in both EUS and BL networks; and identified as "type1_INs" in this paper (Fig. 8 A, Table 1). The DCM contains ~1.7 and the LSCC contains ~1.6 type1_INs per section (Table 2). Cells in which one marker is brightly fluorescent but the other marker is only weakly fluorescent exhibit greenish-yellow or redish-yellow staining in merged images. Cells with this labelling are classified as "type2_INs" (Figs. 5 C, D and 6C, D, 8A, Table 1) and most likely represent a pIN neuron in one circuit and sIN in the other circuit (see circuit diagram in Fig. 8 A).

The DCM has ~0.5 Type 2a, bright green + weak red interneurons per section (i.e., pIN in the EUS circuit and sIN in the BL circuit) and has ~1.4 Type 2b bright red + weak green neurons, i.e. pIN in the BL circuit and sIN in EUS circuit). The LSCC also has 0.8 Type 2a and 1.0 Type2B INs per section (Fig. 7, Table 2). INs exhibiting weak double labeling with each marker and weak yellow staining in merged images (identified as "type3_INs") averaged 4.7 and 2.7 cells per section in DCM and LSCC, respectively; these numbers do not differ significantly from the numbers of type1_INs.

In summary, when cells are grouped according to the type of marker and brightness, the average number of cells per section with each combination of markers is similar in DCM and LSCC (Table 2, Fig. 8B) typically ranging between 0.5 and 7 cells per section. However, the numbers of EUS-sINs in both compartments ranging from 25 to 60 cells per section are significantly higher than all other types. The number of type1_INs that are presumably synaptically connected to both EUS-MNs and SPPNs is roughly similar to the number of type2_INs that have a direct synaptic connection with an output neuron in one circuit and an indirect connection via an interneuron to an output neuron of the other circuit. Merging the numbers of type1_INs and type2_INs yields 3.6 double-labeled neurons per section in DCM and 3.5 such neurons in LSCC. In the DCM type1_INs comprise 20.5 % of all EUS-pINs and 24.2 % of all BL-pINs (Fig. 8Ac - yellow segment). In the LSCC type1_INs comprise ~22 % of all EUS-pINs and ~17 % of all BL-pINs (Fig. 8Ae and Ag - yellow segments). On the other hand, type2_INs represent ~6.3 % of all EUS-pINs and ~20 % of all BL-pINs (Fig. 8Aa - blue segment, Fig. 8Ad - orange segment) in the DCM and ~11 % of both EUS-pINs and BL-pINs In the LSCC (Fig. 8Ae - blue segment, Fig. 8Ag - orange segment). Type3_INs consisting of double-labeled cells which only moderately or weakly express each of the markers, constitute a very small portion (3.2 % and 3.6 %, respectively) of EUS-sINs neurons in the DCM and LSCC (Fig. 8Ab, Af - brown segments) but constitute a large percentage (39 % and 30 %, respectively) of all BL-sINs in both of these compartments (Fig. 8Ad, Ah - brown segments).

Inhibitory neurons in EUS circuitry

To identify inhibitory neurons among EUS-INs we used an antibody against Pax2 (Figs. 9–11). Pax2 is a transcription factor which determines the inhibitory nature of neurons in early development and is expressed in nuclei of GABAergic and glycinergic cells in adult animals (Batista and Lewis, 2008; Huang et al., 2008; Juarez-Morales et al., 2016; Larsson, 2017). The combination of PRV tracing with Pax2 immuno-labeling revealed Pax2-immunoreactivity among 2.73 % of EUS-pINs in DCM and 8.39 % of EUS-pINs in LSCC (Figs. 9 and Fig.12). While the percentage of Pax2-positive cells among EUS-sINs was substantially higher: ~13 % in DCM and 26.7 % in LSCC (Figs. 9–11). The total percentage of colocalization in all types of EUS-related

Table 2
Average numbers of labeled interneurons per section.

Brightness_Marker	DCM M ± SD, n = 3	LSCC M ± SD, n = 3	Welch t-test for significant differences ($\alpha = 0.05$)
B_G	6.01 ± 1.63	4.98 ± 1.99	t(df) = 0.69 < 2.9 = t_{crit}, df = 3.8
B_R	3.87 ± 1.86	2.47 ± 1.37	t(df) = 1.05 < 2.9 = t_{crit}, df = 3.7
B_G + B_R	1.68 ± 1.53	1.63 ± 0.26	t(df) = 0.05 < 4.1 = t_{crit}, df = 2.1
B_G + W_R	0.52 ± 0.3	0.80 ± 0.29	t(df) = 1.16 < 2.7 = t_{crit}, df = 4
B_R + W_G	1.39 ± 0.94	1.05 ± 0.31	t(df) = 0.59 < 3.8 = t_{crit}, df = 2.4
W_G + W_R	4.75 ± 1.8	2.69 ± 0.59	t(df) = 1.88 < 3.8 = t_{crit}, df = 2.4
W_G	38.1 ± 18.5	25 ± 8.25	t(df) = 1.12 < 3.8 = t_{crit}, df = 2.4
W_R	6.91 ± 3.31	5.54 ± 3.15	t(df) = 0.52 < 2.7 = t_{crit}, df = 4

Average numbers of PRV-labeled interneurons (n = 3 rats) in 50 μm thick sections of DCM and LSCC. Neurons are grouped according staining with one or two fluorescent markers and their expression (= brightness). B_G – bright green; B_R – bright red; B_G + B_R – bright yellow, i.e. colocalization of bright green and bright red markers in the same cell; B_G + W_R - bright green and weak or moderate red in the same cell; B_R + W_G – bright red and weak or moderate green in the same cell; W_G + W_R – weak yellow, i.e. weak or moderate green and weak or moderate red in the same cell; W_G – weak or moderate green; W_R - weak or moderate red; t(df) – calculated t value in Welch's t-test; t_{crit} – critical t value; df – calculated degree of freedom. There were no significant differences of means in all groups between DCM and LSCC.

interneurons in the LSCC is 35.1 % in LSCC and 15.7 % in DCM. This suggests that a large majority of EUS-related interneurons in both compartments (64.8 % in LSCC and 84.3 % in DCM) have an excitatory function.

Discussion

To elucidate the spinal circuitry involved in the control of the lower urinary tract (LUT) which consists of multiple organs it is necessary to study not only the organization of circuits that control individual organs, i.e., the bladder, urethra and external urethral sphincter but also the interconnected parts of these circuits that coordinate the functions of the organs. The neural control of LUT is also complicated because it coordinates the activity of autonomic pathways that regulate LUT smooth muscle with activity of somatic motor pathways that regulate striated muscle of the external urethral sphincter (EUS). Thus, the storage and elimination of urine requires the integration of visceral and somatic spinal networks.

The location of EUS-related and bladder-related interneurons in the lumbosacral spinal cord

The present study which used transneuronal tracing techniques to simultaneously label spinal neurons related to the EUS with a green
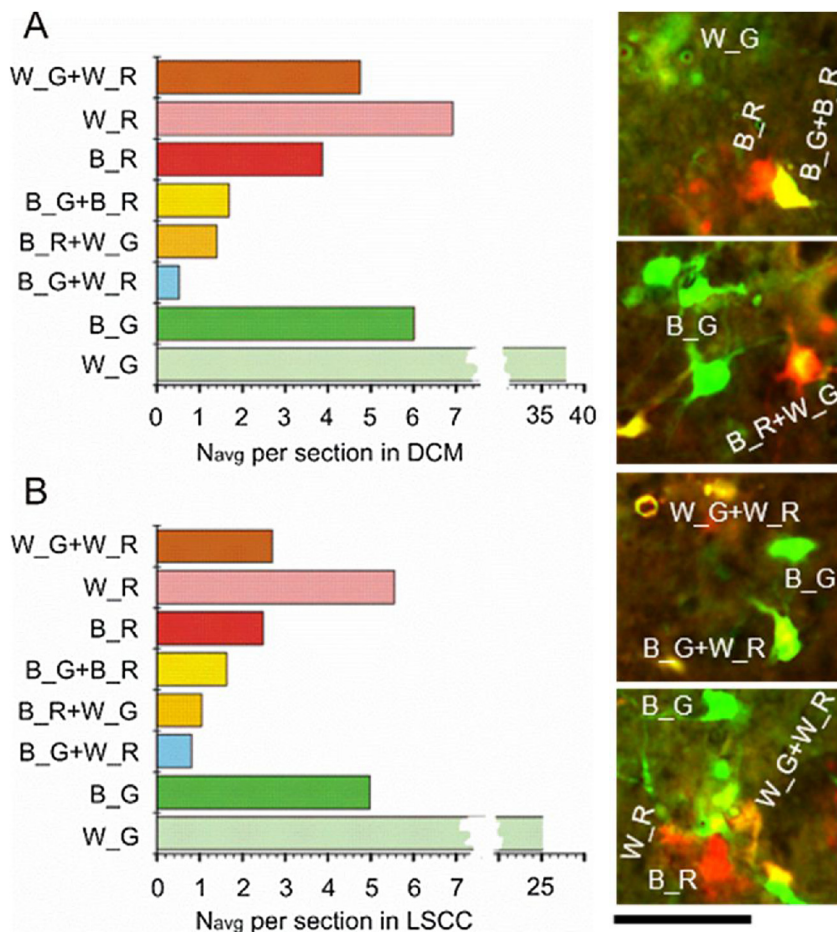

Fig. 7. Bar plots illustrating averaged numbers of each neuron type per 50 μm transverse section (average from data in 3 rats). **A** – neurons counted in DCM (total 7081 cells in 107 sections). **B** – neurons counted in LSCC (total 9488 cells in 206 sections); in *A* and *B* the abscissa is stretched for better resolution. Abbreviations on the ordinate: W_G – moderate or weak green, W_R - moderate or weak red, B_G – bright green, B_R – bright red; "+" designates colocalization of corresponding markers. Images in the right column illustrate labeling by different combinations of expressed markers. Scale bar is 100 μm (For interpretation of the references to colour in this figure legend, the reader is referred to the web version of this article.).
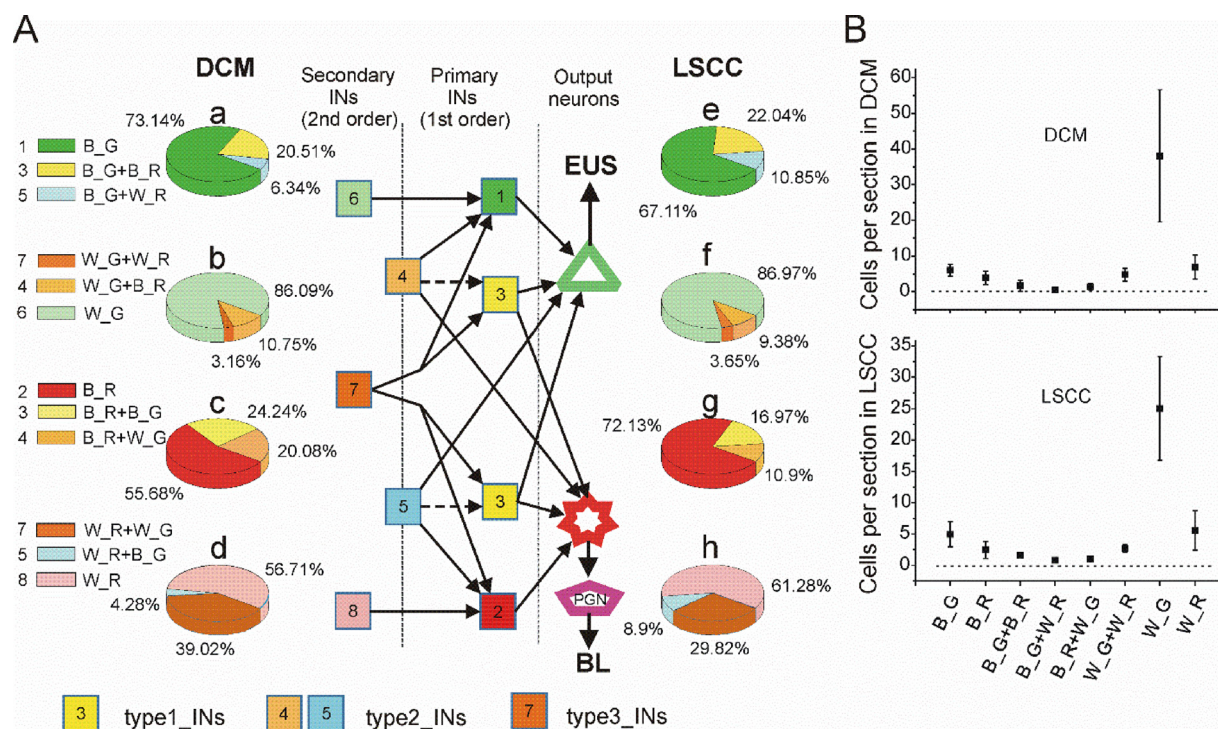
Fig. 8. A - Pie plots illustrating proportions of neurons with colocalized markers relative to the entire populations of four specified classes of labeled neurons: ***a, e*–** EUS-pINs, ***b, f*–** EUS-sINs, ***c, g*** – BL-pINs, ***d, h*** – BL-sINs. Left column – pie plots showing percentages of the specified classes in L6/S1 DCM, right column – pie plots showing percentages of the specified classes in L3/L4 LSCC. Percentage of cells is given next to corresponding segments of pie plots. A circuit diagram of presumed synaptic connections among the EUS-related and BL-related neuronal populations in the DCM and LSSC. Color-coding in the diagram corresponds to color coding in the pie plots. For clarity color coding of the bars on the left and in the legend at the bottom of the figure duplicate numbering of each color; the same colors and numbers were also used for neurons in the circuit diagram. Interneurons with dual staining are divided to 3 types according to combination of expressed markers. All bright yellow neurons are classified as "type1_INs"; cells expressing one bright marker and a weak or moderate other marker are classified as "type2_INs"; double-labeled INs weakly or moderately stained with either marker are classified as "type3_INs". Therefore, type1_INs includes only pINs, type3_INs includes only sINs, whereas type2_INs includes cells which are pINs in one circuit and sINs in the other circuit. Output neurons EUS-MNs and BL-SPPNs depicted as a green triangle and a red star, respectively, were not counted. A peripheral ganglion is depicted as a purple pentagon. **B** – plots of averaged (n = 3 rats) numbers of neurons per 50 μm thick sections calculated for DCM (top) and LSCC (bottom). Abbreviations for names of combination of markers are decoded in the legends for Figs. 3 and 7, and for Table 2. Data are shown as M ± SE (For interpretation of the references to colour in this figure legend, the reader is referred to the web version of this article.).

marker (PRV-GFP) and neurons related to the bladder with a red marker (PRV-RFP) identified several populations of interneurons (INs) at two levels of the lumbosacral spinal cord of rats that are involved in LUT function. Neurons labeled with only one fluorescent marker are assumed to mediate independent control of either the bladder or EUS; while neurons expressing both markers may be involved in simultaneous control and coordination of the bladder and EUS. Neurons of both types were identified in the L3-L4 and L6-S1 spinal segments supporting previous proposals that intersegmental communication between interneuronal circuitry in the L3-L4 lumbar spinal coordinating center (LSCC) and the efferent output neurons (i.e., EUS motoneurons and bladder parasympathetic preganglionic neurons) in the L6-S1 spinal cord contributes to the neural regulation of the lower urinary tract (Fig. 3).

Identification of double labelled interneurons involved in bladder and EUS circuitry

Dual PRV tracing aimed at detecting double-labeled spinal neurons after injection of different PRV strains into two different peripheral targets raises a question of whether a neuron can be infected by two viruses simultaneously and whether a time lag between the expression of two viruses due to differences in virus transport, invasiveness, replication or progression of infection can affect the efficiency of dual labelling (Cano et al., 2004; Jansen et al., 1995; Nadelhaft et al., 2002; Nadelhaft and Vera, 2001; Ter Horst, 2000; Xu et al., 2006). The creators of PRV614 encoding RFP have shown that DRG neurons

infected simultaneously with PRV512 and PRV614 were 100 % double labeled (Banfield et al., 2003). However, with a 2 h or 4 h interval between injections only ~25–30 % and 1–3 % of neurons, respectively, expressed colocalized markers. No double labeling was observed with a 6 h interval. This suggests a limitation for parallel tracing because a significant amount of superinfection inhibition occurs prior to 2 h post-infection.

The issue of superinfection inhibition was a potential problem in the present experiments because of the difference in peripheral neuroanatomy of the EUS and bladder innervation (i.e., the existence of a synapse in the bladder parasympathetic ganglia) which would delay the transport of virus to the bladder output neurons in the spinal cord. This could be compensated for by injecting the virus into the bladder earlier. However this would require two successive surgeries within 12 − 24 hours, which would be stressful for an animal. Another way to equalize labelling by two viruses with different invasive properties is to increase the number of particles of the weaker virus injected into a target organ (Cano et al., 2004) in order to increase probability of virus uptake by presynaptic boutons and the number of axons transporting the virus. This method was used in the present experiments to enhance labelling in the BL circuit by increasing the volume of PRV614 injected to the BL wall 1.3–1.5 times above the volume of PRV512 injected simultaneously into the EUS. This increase in volume was effective in producing similar PRV expression at the same post-infection time point in single and double labelled BL– and EUS-related INs although it should be noted that the number of BL-related INs was smaller than the number of EUS-related INs. This difference could be due to the smaller
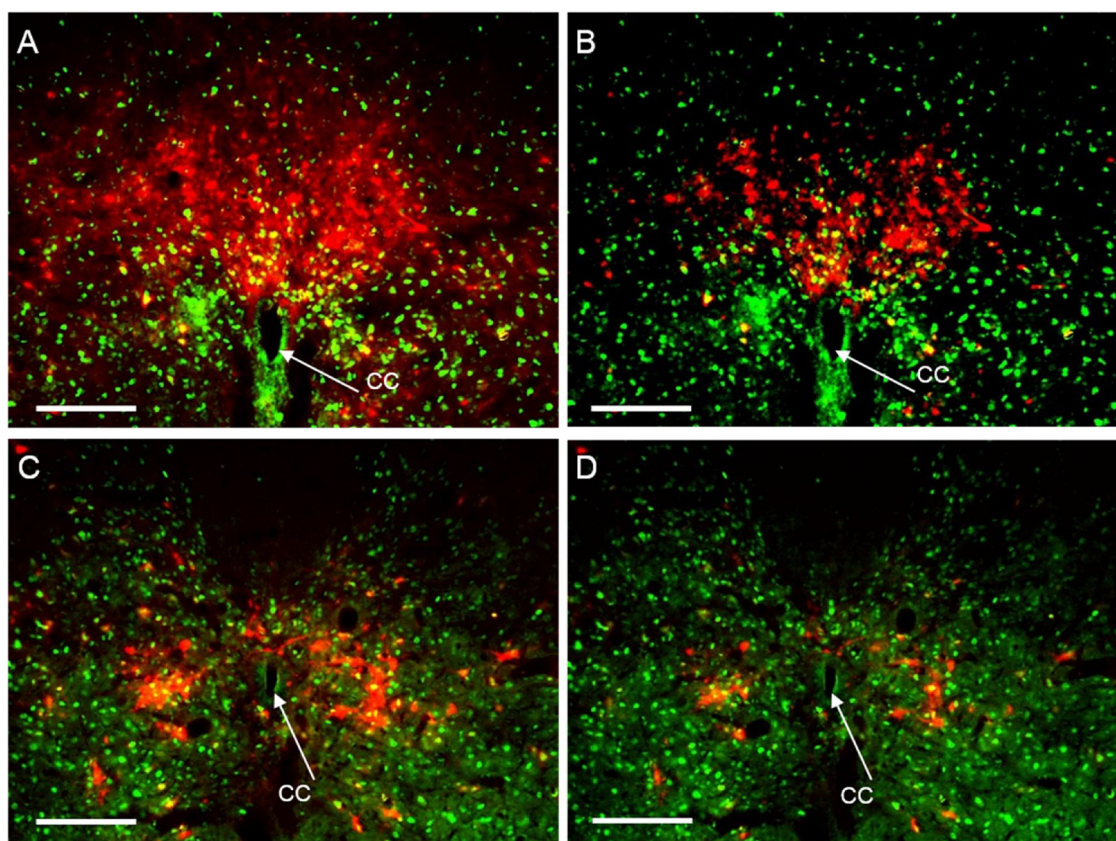
Fig. 9. *A, B* – RFP-labeled EUS-INs in DCM photographed with long (*A*) and short (*B*) exposures. *C, D* – RFP-labeled EUS-INs in LSSC photographed with long (*C*) and short (*D*) exposures. Pax2 immunostaining (green) revealed nuclei of inhibitory neurons. Yellow dots designate colocalization of the two markers. Thus, red cells with yellow nuclei are presumed to be EUS-related inhibitory interneurons. Scale bars are 200 μm (For interpretation of the references to colour in this figure legend, the reader is referred to the web version of this article.).

number of INs in the BL network because this difference was observed in single labelling experiments in rats (Nadelhaft and Vera, 1996; Nadelhaft et al., 1992).

However, even if the numbers of BL-related neurons are low due to a delay in virus transport and post-infection suppression of expression, our data still demonstrate a substantial convergence of BL and EUS interneuronal circuitry exhibiting bright fluorescence, (i.e., ~26 % of all EUS-pINs in the DCM and ~33 % in the LSCC are involved in both EUS and BL circuitry) (Fig. 8Aa, Ae). Among the BL-pINs the co-labelling is not markedly different in the DCM (~44 %) and in the LSCC (~28 %) (Fig. 8Ac, Ag). These percentages are substantially higher than the percentage of BL-EUS double labelling with PRV in the DCM in adult rats (Nadelhaft, et al., 2002) which may be related to the younger age of our animals.

Identification of first order and second order interneurons

To assess the organization of the multiple neural networks involved in the control of LUT function we evaluated not only PRV labelling from a single organ and dual labelling from two organs but also the variation in the intensity of labelling, which should distinguish pINs from sINs that are two or more synapses upstream from the output neurons in L6-S1 (see Fig. 3A). The rationale underlying the use of this method is based on the ability of the attenuated "PRV Bartha" strain to propagate transneuronally in the retrograde direction (Pickard et al., 2002) through a chain of synaptically connected neurons (Enquist, 2002; Enquist et al., 2002; Husak et al., 2000) and that viral expression is delayed after passage across each synapse. It is reasonable therefore to expect that at short post-infection times the position of a neuron in a chain can be roughly estimated by the intensity of its fluorescence in

comparison with fluorescence of its neighbors in the same network: i.e., dim fluorescence reflecting the beginning of expression in 2nd or 3rd order sINs, while bright fluorescence reflects earlier full expression in 1st order pINs that directly synapse with output neurons (Fig. 3). Thus, several factors including time after injection of the virus are important in interpreting the results of transneuronal labelling experiments. Previous studies that used PRV tracing to examine the neural pathways involved in micturition in rats (Nadelhaft et al., 2002; Nadelhaft and Vera, 1996, 2001; Nadelhaft et al., 1992; Sugaya et al., 1997; Vizzard et al., 1995; Yu et al., 2003) reported that spinal output neurons traced from EUS and BL were identified in L6/S1 Onuf's nucleus and in the IML nucleus 2.5–3 days post-inoculation, and that after a 12−24 h longer survival time populations of labeled segmental interneurons were identified in the DCM. Although the location of INs in the DCM is similar in the various reports, the number of labeled INs in the DCM varied apparently due to differences in the titer of the virus, different labeling criteria, variations in age and sex of animals, etc. Our experiments which were performed on ~P30 juvenile male rats without fully mature spinal circuitry but still capable of independent urination (de Groat et al., 1998; Maggi et al., 1986; Zvarova and Zvara, 2012) identified larger numbers of LUT-related INs in the DCM than those previously reported. This increase in numbers could be due to immaturity because PRV tracings from another muscle in the pelvis (the levator ani) in 30 day-old and in adult rats showed that the number of labeled INs in the DCM in young animals is twice as large as in adult rats presumably due to more profound axonal arborizations and a higher number of non-specific synaptic contacts in adolescents (Dobberfuhl et al., 2014). In preliminary experiments (unpublished observation) we found a similar age dependence for numbers of neurons traced in DCM and LSCC from the EUS. Therefore, it is likely that
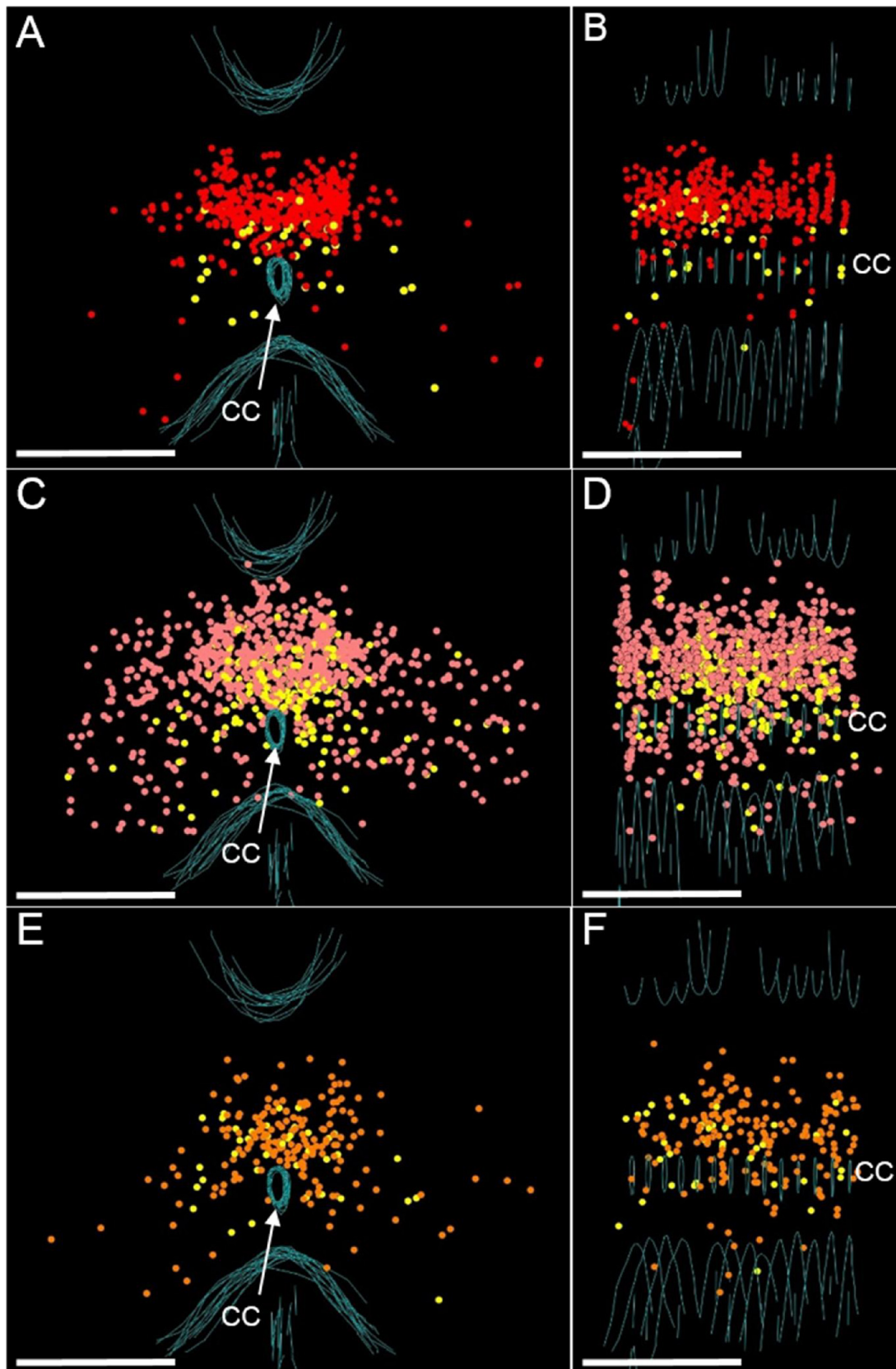
Fig. 10. Set of maps (n = 14 sections) with RFP-labeled EUS-INs in the DCM immuno-stained for Pax2 (Pax2⁺ cells have GFP-labeled nuclei). Left column – transverse view, right column – side view. **A, B** – Pax2-negative EUS-pINs depicted by red dots and EUS-pINs with Pax2-positive nuclei depicted by yellow dots. **C, D** – in the same DCM Pax2-negative EUS-sINs depicted by pink dots and EUS-sINs with Pax2-positive nuclei depicted by yellow dots. **E, F** – superimposed populations of Pax2⁺ EUS-pINs (yellow) and Pax2⁺ EUS-sINs (orange). Scale bars are 500 μm (For interpretation of the references to colour in this figure legend, the reader is referred to the web version of this article.).
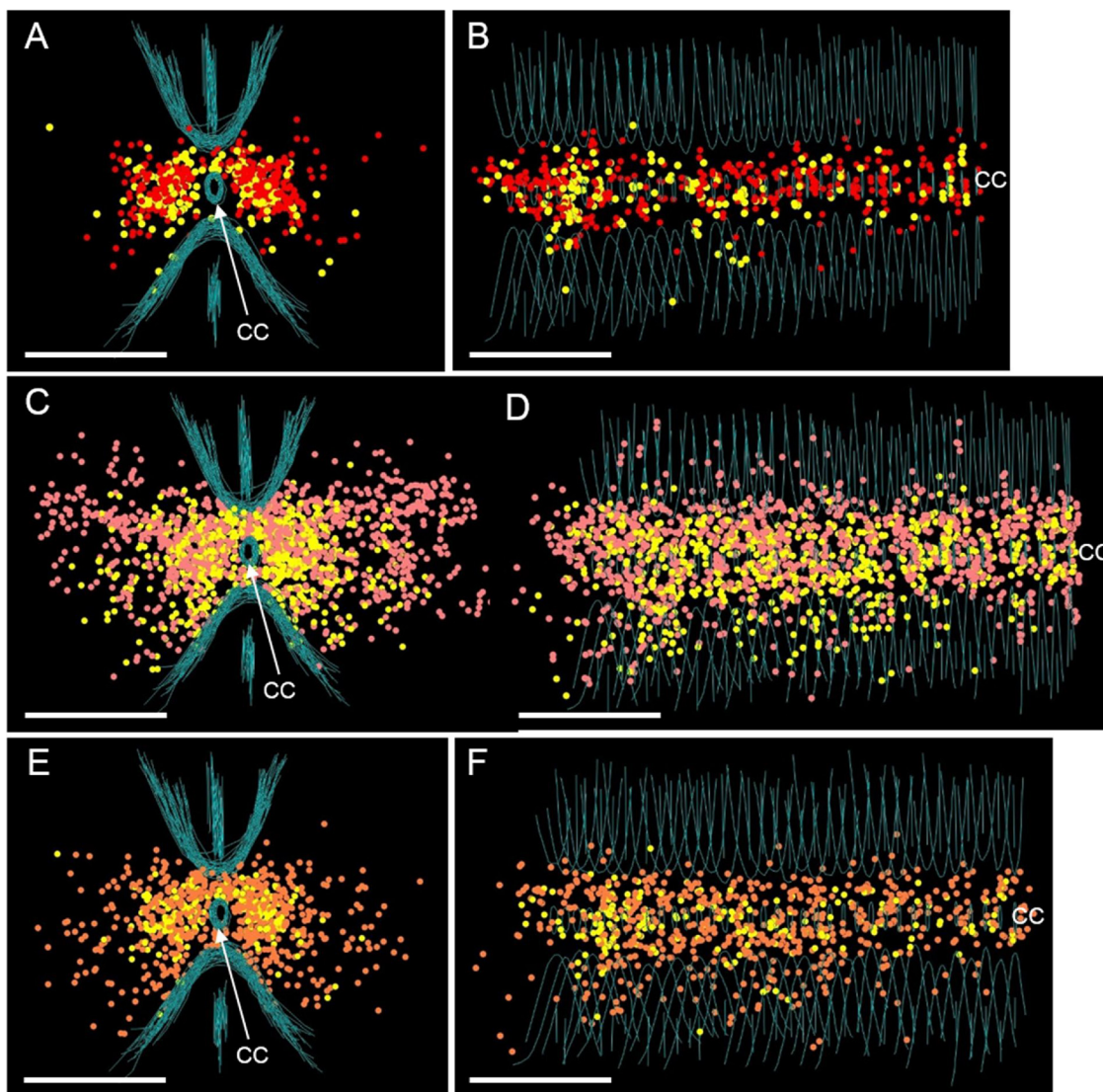
Fig. 11. Similar set of maps (n = 36 sections) for RFP-labeled EUS-INs in the LSSC and immuno-stained for Pax2. Color coding and section orientation are the same as in Fig. 10. Scale bars are 500 μm.
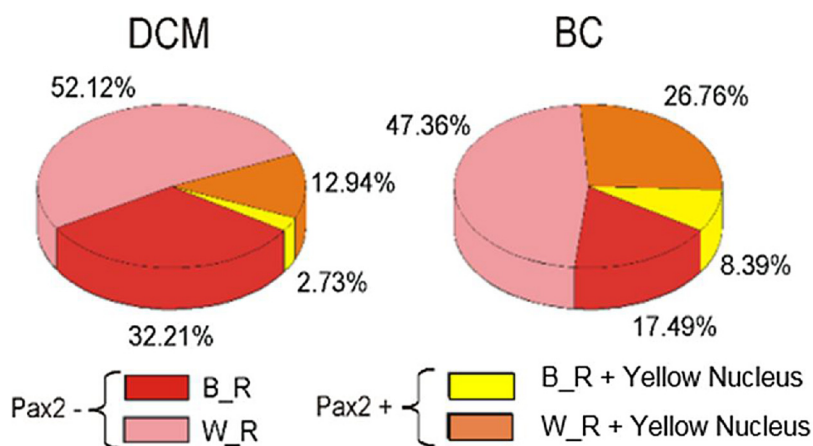

Fig. 12. Pie plots illustrating proportions of Pax2-positive neurons among the whole PRV-RFP labeled populations of EUS-INs in the DCM (left) and LSSC (right). Note lower representation of putative inhibitory neurons in the DCM as compared to LSSC.

LUT-related spinalnetworks in ~P30 juvenile male rats represent an intermediate developmental stage between newborn pups and adult (> P60) animals.

Identification of propriospinal neurons projecting from the LSCC in L3-L4 to the L6-S1 circuitry controlling the lower urinary tract

The intersegmental communication between the L3-L4 LSCC and L6-S1 levels of the spinal cord is mediated by a special kind of interneuron termed a propriospinal neuron which has an essential role in the generation of EUS bursting in rats after thoracic spinal cord transection (Chang et al., 2007). EUS bursting reflects rhythmic contractions and relaxations of the EUS which are necessary for efficient voiding in rats (Kadekawa et al., 2016; Yoshiyama et al., 2000).Therefore the LSCC is potentially an important component of the spinal mechanisms that coordinate bladder and EUS functions. A significant impact of LSCC on EUS-MNs modulation is also suggested by the profound axonal arborization of axons descending from L3/L4 to the location of EUS-MNs in the ventral horn of L6/S1 (Fig. 4).

Our PRV tracing studies identified populations of L3-L4 INs that must contribute to this intersegmental EUS bursting mechanism. Some LSCC INs exhibit bright green fluorescence after PRV labelling and therefore according to our working hypothesis (see discussion above) are propriospinal primary interneurons that directly synapse with the EUS motoneurons (Fig. 3). This conclusion is also supported indirectly by the expression of PRV in these L3/L4 LSCC propriospinal neurons at approximately the same time as it occurs more caudally in the L6/S1 DCM which contains segmental pINs that synapse with EUS motoneurons. Indirect evidence that segmental DCM inhibitory neurons synapse with EUS-MNs has been published by Holstege and coworkers (Blok et al., 1997, 1998; Sie et al., 2001). While the early onset of intense PRV expression in LSCC neurons suggests that they are neurons directly synapsing with EUS MNs, it is important to acknowledge that bright fluorescence might also occur in other types of LSCC neurons due to differences in rate of virus transport or GFP expression in cells of different types and sizes or differences in the number of synaptic contacts and distances between cells. Thus some brightly fluorescent LSCC neurons may not project directly to EUS MNs but rather may be propriospinal neurons that project to INs in the L6-S1 DCM that in turn make synaptic connections with EUS MNs. These neurons would then be classified as secondary interneurons (sINs). Additionally, some brightly fluorescent LSCC neurons might not be propriospinal neurons but rather segmental INs that synapse with the LSCC propriospinal neurons. Thus the number of genuine propriospinal neurons in the LSCC may be lower than the number of pINs in our estimates. Nevertheless, absolute numbers of EUS-pINs in the DCM and LSCC are very similar (Fig. 8A) suggesting that the contribution of direct inputs to EUS MNs from the LSCC is similar to the inputs from the DCM, which is a well-established site of interneuronal control of lower urinary tract function (de Groat et al., 2015).

Approximately one quarter of the brightly green fluorescent EUS-related INs in the LSCC also exhibit bright red fluorescence indicating their involvement in the control of bladder function. (Fig. 8A). Some of these double labeled neurons are likely to be propriospinal neurons that simultaneously modulate the activity of bladder and EUS output neurons in L6-S1 spinal cord; and therefore must be an important part of the spinal mechanism for coordinating the activity of the two organs. More direct evidence for the existence of propriospinal neurons in the LSCC was obtained in our recent electrophysiological and anatomical experiments (Karnup and de Groat, 2020) which showed that electrical stimulation in the ventral column elicited antidromic spikes in EUS-related INs located in the LSCC. Additionally, when neurons were reconstructed after filling with biocytin, some exhibited axons projecting into the ventral column where they presumably pass caudally to L6-S1 to synapse with neurons in the LUT-related circuitry.

The function of propriospinal neurons and segmental interneurons in the LSCC

An important question that remains is: do labelled propriospinal neurons in the LSCC send excitatory or inhibitory signals to the LUT-related neurons in L6/S1? While we have not identified the neurotransmitters in bladder-related or co-labeled LSCC neurons, we have shown that approximately 8% of single labelled EUS-related pINs in the LSCC express Pax2 immunoreactivity (Figs. 9–11), a marker for spinal GABAergic and glycinergic inhibitory neurons (Balazs et al., 2017; Batista and Lewis, 2008; Huang et al., 2008; Larsson, 2017; Ross et al., 2010). The remainder of these neurons are presumably excitatory. It will be important in future experiments to determine if the subpopulation of co-labelled pINs in L3-L4 also express Pax2 immunoreactivity and therefore are inhibitory. If this can be demonstrated it would indicate that there must be at least two pathways, one excitatory and one inhibitory that project from the LSCC to the EUS motoneurons and bladder preganglionic neurons in L6-S1. The possible existence of two opposing inputs from the LSCC to EUS motoneurons is important because it could underlie the EUS bursting that consists of active periods and intervening silent periods. Alternating inputs to the EUS motoneurons from the putative excitatory and inhibitory pINs in the LSCC could contribute to the EUS bursting.

In contrast to the low percentage of Pax2 positive brightly fluorescent pINs in the LSCC a larger percentage (26 %) of weakly fluorescent sINs in the LSCC exhibit Pax2 staining. This population could represent local inhibitory neurons or second order propriospinal neurons (see discussion above) that send inhibitory input to the L6-S1 DCM. In our previous experiments conducted in spinal slices biocytin filling of EUS-related neurons in the LSCC revealed local interneurons with non-branching or poorly branching axons restricted to the region of the LSCC. The possible function of these interneurons was evaluated by recording the synaptic responses of EUS-related LSCC neurons while electrically stimulating the spinal slice at different distances and directions from the recorded cell. The responses were almost exclusively excitatory while inhibitory responses were rare, weak and unstable. This suggests that the Pax2 positive, putative inhibitory population of sINs in the LSCC projects beyond the LSCC and may project to the DCM in the L6-S1 spinal cord where it could act to suppress tonic EUS activity and contribute to EUS bursting (see below).

Segmental interneurons in L6-S1 that may contribute to EUS bursting or inhibition of EUS activity during voiding

Relaxation of the EUS during voiding requires suppression of EUS-MN activity by inhibitory interneurons participating in the micturition reflex. Some evidence indicates that these neurons are located in the L6/S1 DCM and are activated by descending input from the pontine micturition center in spinal cord intact animals (Blok et al., 1997; Buss and Shefchyk, 2003; Sie et al., 2001). We used immunoreaction for Pax2 which is expressed in GABAergic as well as in glycinergic neurons (Batista and Lewis, 2008; Huang et al., 2008; Juarez-Morales et al., 2016; Larsson, 2017) to determine if EUS-related interneurons in the DCM are inhibitory. Surprisingly, among this population the number of inhibitory neurons colocalizing bright PRV-RFP staining with Pax2 expression was very low, approximately 3% of the whole pool (Fig. 12). A larger percentage (~13 %) of sINs with weaker RFP labeling and which probably do not directly synapse with EUS-MNs exhibited Pax2 IR. Thus, an interaction between weak segmental inhibitory input from the DCM and inhibitory propriospinal input from the L3/L4 LSCC, which also contains Pax2 positive primary and secondary inhibitory INs may be necessary to produce the relaxation phase of EUS bursting.

Segmental interneurons in L6-S1 that contribute to tonic EUS activity

Although EUS bursting is eliminated after transection of the spinal

cord at the L4-L5 level which blocks input from the LSCC to L6-S1; this lesion does not eliminate tonic EUS activity which contributes to closure of the urethral outlet during urine storage. Thus, EUS tonic activity which is triggered by afferent input from the bladder (de Groat et al., 2015) must be mediated by a reflex pathway organized in the L6-S1 spinal cord. Based on the long latency of the bladder to EUS reflex after transection of the cord at the L4-L5 level (Chang et al., 2007) the pathway cannot be monosynaptic and therefore must be mediated by INs. The IN relay station involved in this pathway is presumably located among the population of PRV–labelled, EUS-related INs identified in this study in the L6-S1 DCM. Some of the DCM INs were brightly fluorescent and therefore according to our criteria were pINs directly synapsing with the EUS motoneurons, while others were less bright sINs that must communicate indirectly with EUS motoneurons by synapsing with the aforementioned pINs. Thus, it seems reasonable to speculate that primary afferent input from the bladder to these two populations of INs in the DCM can generate tonic EUS activity via multisynaptic circuits involving excitatory pINs and sINs.

In summary, our data suggest that the LSCC located dorsal and lateral to the central canal in the L3/L4 spinal segments represents a significant portion of the spinal circuitry controlling the LUT. Some of the brightly fluorescent neurons (termed pINs) in the LSCC are presumed to be propriospinal neurons projecting to the LUT motoneurons or possibly to interneuronal circuitry in the DCM of the L6-S1 spinal segments. The presence of Pax2, a marker for GABAergic and glycinergic inhibitory neurons in a subpopulation of LSCC EUS pINs raises the possibility that propriospinal pathways from the LSCC to L6-S1 mediate inhibitory as well as excitatory influences on EUS function. Although the LSCC and the DCM have a similar pattern of distribution of LUT sINs and pINs, the larger number of EUS-sINs in both DCM and LSCC compared to number of BL-sINs suggests that the interneuronal control of the EUS is more complex than that of the bladder.

Ethical statement

Author contributions

W.C.deG.- conception and design of research, edited the manuscript; S.V.K.- performed experiments, analyzed data, prepared figures, drafted manuscript.

Conflicts of interest

No conflict of interests, financial or otherwise, are declared by the authors.

Acknowledgements

References

superficial spinal dorsal horn. Brain Struct. Funct. 222, 2157–2171.

Banfield, B.W., Kaufman, J.D., Randall, J.A., Pickard, G.E., 2003. Development of pseudorabies virus strains expressing red fluorescent proteins: new tools for multisynaptic labeling applications. J. Virol. 77, 10106–10112.

Barbe, M.F., Gomez-Amaya, S.M., Salvadeo, D.M., Lamarre, N.S., Tiwari, E., Cook, S., Glair, C.P., Jang, D.H., et al., 2018. Clarification of the innervation of the bladder, external urethral sphincter and clitoris: a neuronal tracing study in female mongrel hound dogs. Anat. Rec. (Hoboken) 301, 1426–1441.

Batista, M.F., Lewis, K.E., 2008. Pax2/8 act redundantly to specify glycinergic and GABAergic fates of multiple spinal interneurons. Dev. Biol. 323, 88–97.

Bienkowski, M.S., Wendel, E.S., Rinaman, L., 2013. Organization of multisynaptic circuits within and between the medial and the central extended amygdala. J. Comp. Neurol. 521, 3406–3431.

Blok, B.F., de Weerd, H., Holstege, G., 1997. The pontine micturition center projects to sacral cord GABA immunoreactive neurons in the cat. Neurosci. Lett. 233, 109–112.

Blok, B.F., van Maarseveen, J.T., Holstege, G., 1998. Electrical stimulation of the sacral dorsal gray commissure evokes relaxation of the external urethral sphincter in the cat. Neurosci. Lett. 249, 68–70.

Buss, R.R., Shefchyk, S.J., 2003. Sacral dorsal horn neurone activity during micturition in the cat. J. Physiol. 551, 387–396.

Cano, G., Sved, A.F., Rinaman, L., Rabin, B.S., Card, J.P., 2001. Characterization of the central nervous system innervation of the rat spleen using viral transneuronal tracing. J. Comp. Neurol. 439, 1–18.

Cano, G., Card, J.P., Sved, A.F., 2004. Dual viral transneuronal tracing of central autonomic circuits involved in the innervation of the two kidneys in rat. J. Comp. Neurol. 471, 462–481.

Card, J.P., Dubin, J.R., Whealy, M.E., Enquist, L.W., 1995. Influence of infectious dose upon productive replication and transynaptic passage of pseudorabies virus in rat central nervous system. J. Neurovirol. 1, 349–358.

Chang, H.Y., Cheng, C.L., Chen, J.J., de Groat, W.C., 2007. Serotonergic drugs and spinal cord transections indicate that different spinal circuits are involved in external urethral sphincter activity in rats. Am. J. Physiol. Renal Physiol. 292, F1044–1053.

Cheng, C.L., de Groat, W.C., 2010. Role of 5-HT1A receptors in control of lower urinary tract function in anesthetized rats. Am. J. Physiol. Renal Physiol. 298, F771–778.

Cheng, C.L., Chai, C.Y., de Groat, W.C., 1997. Detrusor-sphincter dyssynergia induced by cold stimulation of the urinary bladder of rats. Am. J. Physiol. 272, R1271–1282.

de Groat, W.C., Araki, I., Vizzard, M.A., Yoshiyama, M., Yoshimura, N., Sugaya, K., Tai, C., Roppolo, J.R., 1998. Developmental and injury induced plasticity in the micturition reflex pathway. Behav. Brain Res. 92, 127–140.

de Groat, W.C., Griffiths, D., Yoshimura, N., 2015. Neural control of the lower urinary tract. Compr. Physiol. 5, 327–396.

Dobberfuhl, A.D., Oti, T., Sakamoto, H., Marson, L., 2014. Identification of CNS neurons innervating the levator ani and ventral bulbospongiosus muscles in male rats. J. Sex. Med. 11, 664–677.

Enquist, L.W., 2002. Exploiting circuit-specific spread of pseudorabies virus in the central nervous system: insights to pathogenesis and circuit tracers. J. Infect. Dis. 186 (Suppl 2), S209–214.

Enquist, L.W., Tomishima, M.J., Gross, S., Smith, G.A., 2002. Directional spread of an alpha-herpesvirus in the nervous system. Vet. Microbiol. 86, 5–16.

Gao, G., Zhang, F., Sun, H.J., Liu, T.Y., Ding, L., Kang, Y.M., Zhu, G.Q., Zhou, Y.B., 2014. Transneuronal tracing of central autonomic regions involved in cardiac sympathetic afferent reflex in rats. J. Neurol. Sci. 342, 45–51.

Guo, F., Li, S., Caglar, M.U., Mao, Z., Liu, W., Woodman, A., Arnold, J.J., Wilke, C.O., et al., 2017. Single-cell virology: on-chip investigation of viral infection dynamics. Cell Rep. 21, 1692–1704.

Hillyer, P., Shepard, R., Uehling, M., Krenz, M., Sheikh, F., Thayer, K.R., Huang, L., Yan, L., et al., 2018. Differential responses by human respiratory epithelial cell lines to respiratory syncytial virus reflect distinct patterns of infection control. J. Virol. 92.

Huang, M., Huang, T., Xiang, Y., Xie, Z., Chen, Y., Yan, R., Xu, J., Cheng, L., 2008. Ptf1a, Lbx1 and Pax2 coordinate glycinergic and peptidergic transmitter phenotypes in dorsal spinal inhibitory neurons. Dev. Biol. 322, 394–405.

Husak, P.J., Kuo, T., Enquist, L.W., 2000. Pseudorabies virus membrane proteins gI and gE facilitate anterograde spread of infection in projection-specific neurons in the rat. J. Virol. 74, 10975–10983.

Jansen, A.S., Nguyen, X.V., Karpitskiy, V., Mettenleiter, T.C., Loewy, A.D., 1995. Central command neurons of the sympathetic nervous system: basis of the fight-or-flight response. Science 270, 644–646.

Jovanovic, K., Pastor, A.M., O'Donovan, M.J., 2010. The use of PRV-Bartha to define premotor inputs to lumbar motoneurons in the neonatal spinal cord of the mouse. PLoS One 5, e11743.

Juarez-Morales, J.L., Schulte, C.J., Pezoa, S.A., Vallejo, G.K., Hilinski, W.C., England, S.J., de Jager, S., Lewis, K.E., 2016. Evx1 and Evx2 specify excitatory neurotransmitter fates and suppress inhibitory fates through a Pax2-independent mechanism. Neural Dev. 11, 5.

Kadekawa, K., Yoshimura, N., Majima, T., Wada, N., Shimizu, T., Birder, L.A., Kanai, A.J., de Groat, W.C., et al., 2016. Characterization of bladder and external urethral activity in mice with or without spinal cord injury–a comparison study with rats. Am. J. Physiol. Regul. Integr. Comp. Physiol. 310, R752–758.

Karnup, S.V., de Groat, W.C., 2020. Propriospinal neurons of L3-L4 segments involved in control of the rat external urethral sphincter. Neuroscience 425, 12–28.

Kim, E.S., Li, H., McCulloch, P.F., Morrison, L.A., Yoon, K.W., Xu, X.M., 2000. Spatial and temporal patterns of transneuronal labeling in CNS neurons after injection of pseudorabies virus into the sciatic nerve of adult rats. Brain Res. 857, 41–55.

Kruse, M.N., Belton, A.L., de Groat, W.C., 1993. Changes in bladder and external urethral sphincter function after spinal cord injury in the rat. Am. J. Physiol. 264, R1157–1163.

Balazs, A., Meszar, Z., Hegedus, K., Kenyeres, A., Hegyi, Z., Docs, K., Antal, M., 2017. Development of putative inhibitory neurons in the embryonic and postnatal mouse

Larsson, M., 2017. Pax2 is persistently expressed by GABAergic neurons throughout the adult rat dorsal horn. Neurosci. Lett. 638, 96–101.

Lee, J.W., Erskine, M.S., 2000. Pseudorabies virus tracing of neural pathways between the uterine cervix and CNS: effects of survival time, estrogen treatment, rhizotomy, and pelvic nerve transection. J. Comp. Neurol. 418, 484–503.

Maggi, C.A., Santicioli, P., Meli, A., 1986. Postnatal development of micturition reflex in rats. Am. J. Physiol. 250, R926–931.

Marson, L., McKenna, K.E., 1996. CNS cell groups involved in the control of the ischiocavernosus and bulbospongiosus muscles: a transneuronal tracing study using pseudorabies virus. J. Comp. Neurol. 374, 161–179.

Metts, B.A., Kaufman, G.D., Perachio, A.A., 2006. Polysynaptic inputs to vestibular efferent neurons as revealed by viral transneuronal tracing. Exp. Brain Res. 172, 261–274.

Nadelhaft, I., Vera, P.L., 1996. Neurons in the rat brain and spinal cord labeled after pseudorabies virus injected into the external urethral sphincter. J. Comp. Neurol. 375, 502–517.

Nadelhaft, I., Vera, P.L., 2001. Separate urinary bladder and external urethral sphincter neurons in the central nervous system of the rat: simultaneous labeling with two immunohistochemically distinguishable pseudorabies viruses. Brain Res. 903, 33–44.

Nadelhaft, I., Vera, P.L., Card, J.P., Miselis, R.R., 1992. Central nervous system neurons labelled following the injection of pseudorabies virus into the rat urinary bladder. Neurosci. Lett. 143, 271–274.

Nadelhaft, I., Miranda-Sousa, A.J., Vera, P.L., 2002. Separate urinary bladder and prostate neurons in the central nervous system of the rat: simultaneous labeling with two immunohistochemically distinguishable pseudorabies viruses. BMC Neurosci. 3, 8.

Pickard, G.E., Smeraski, C.A., Tomlinson, C.C., Banfield, B.W., Kaufman, J., Wilcox, C.L., Enquist, L.W., Sollars, P.J., 2002. Intravitreal injection of the attenuated pseudorabies virus PRV Bartha results in infection of the hamster suprachiasmatic nucleus only by retrograde transsynaptic transport via autonomic circuits. J. Neurosci. 22, 2701–2710.

Qin, C., Farber, J.P., Foreman, R.D., 2007a. Spinal cord stimulation modulates activity of lumbosacral spinal neurons receiving input from urinary bladder in rats. Neurosci. Lett. 428, 38–42.

Qin, C., Lehew, R.T., Khan, K.A., Wienecke, G.M., Foreman, R.D., 2007b. Spinal cord stimulation modulates intraspinal colorectal visceroreceptive transmission in rats. Neurosci. Res. 58, 58–66.

Ross, S.E., Mardinly, A.R., McCord, A.E., Zurawski, J., Cohen, S., Jung, C., Hu, L., Mok, S.I., et al., 2010. Loss of inhibitory interneurons in the dorsal spinal cord and elevated itch in Bhlhb5 mutant mice. Neuron 65, 886–898.

Schramm, L.P., Strack, A.M., Platt, K.B., Loewy, A.D., 1993. Peripheral and central pathways regulating the kidney: a study using pseudorabies virus. Brain Res. 616, 251–262.

Sie, J.A., Blok, B.F., de Weerd, H., Holstege, G., 2001. Ultrastructural evidence for direct projections from the pontine micturition center to glycine-immunoreactive neurons in the sacral dorsal gray commissure in the cat. J. Comp. Neurol. 429, 631–637.

Sugaya, K., Roppolo, J.R., Yoshimura, N., Card, J.P., de Groat, W.C., 1997. The central neural pathways involved in micturition in the neonatal rat as revealed by the injection of pseudorabies virus into the urinary bladder. Neurosci. Lett. 223, 197–200.

Taylor, M.P., Kobiler, O., Enquist, L.W., 2012. Alphaherpesvirus axon-to-cell spread involves limited virion transmission. Proc. Natl. Acad. Sci. U. S. A. 109, 17046–17051.

Ter Horst, G.J., 2000. Transneuronal retrograde dual viral labelling of central autonomic circuitry: possibilities and pitfalls. Auton. Neurosci. 83, 134–139.

Truitt, W.A., Coolen, L.M., 2002. Identification of a potential ejaculation generator in the spinal cord. Science 297, 1566–1569.

Vizzard, M.A., Erickson, V.L., Card, J.P., Roppolo, J.R., de Groat, W.C., 1995. Transneuronal labeling of neurons in the adult rat brainstem and spinal cord after injection of pseudorabies virus into the urethra. J. Comp. Neurol. 355, 629–640.

Xu, C., Giuliano, F., Yaici, E.D., Conrath, M., Trassard, O., Benoit, G., Verge, D., 2006. Identification of lumbar spinal neurons controlling simultaneously the prostate and the bulbospongiosus muscles in the rat. Neuroscience 138, 561–573.

Yoshiyama, M., deGroat, W.C., Fraser, M.O., 2000. Influences of external urethral sphincter relaxation induced by alpha-bungarotoxin, a neuromuscular junction blocking agent, on voiding dysfunction in the rat with spinal cord injury. Urology 55, 956–960.

Yu, X., Xu, L., Zhang, X.D., Cui, F.Z., 2003. Effect of spinal cord injury on urinary bladder spinal neural pathway: a retrograde transneuronal tracing study with pseudorabies virus. Urology 62, 755–759.

Zvarova, K., Zvara, P., 2012. Urinary bladder function in conscious rat pups: a developmental study. Am. J. Physiol. Renal Physiol. 302, F1563–1568.